Electronic Supplementary Material (ESI) for Dalton Transactions.

Halogenated isophthalamides and dipicolineamides: the role of the halogen substituent on the anion binding properties

Giacomo Picci, Carla Bazzicalupi, Simon J. Coles, Paola Gratteri, Francesco Isaia, Vito Lippolis, Riccardo Montis, Sergio Murgia, Alessio Nocentini, James B. Orton, and Claudia Caltagirone

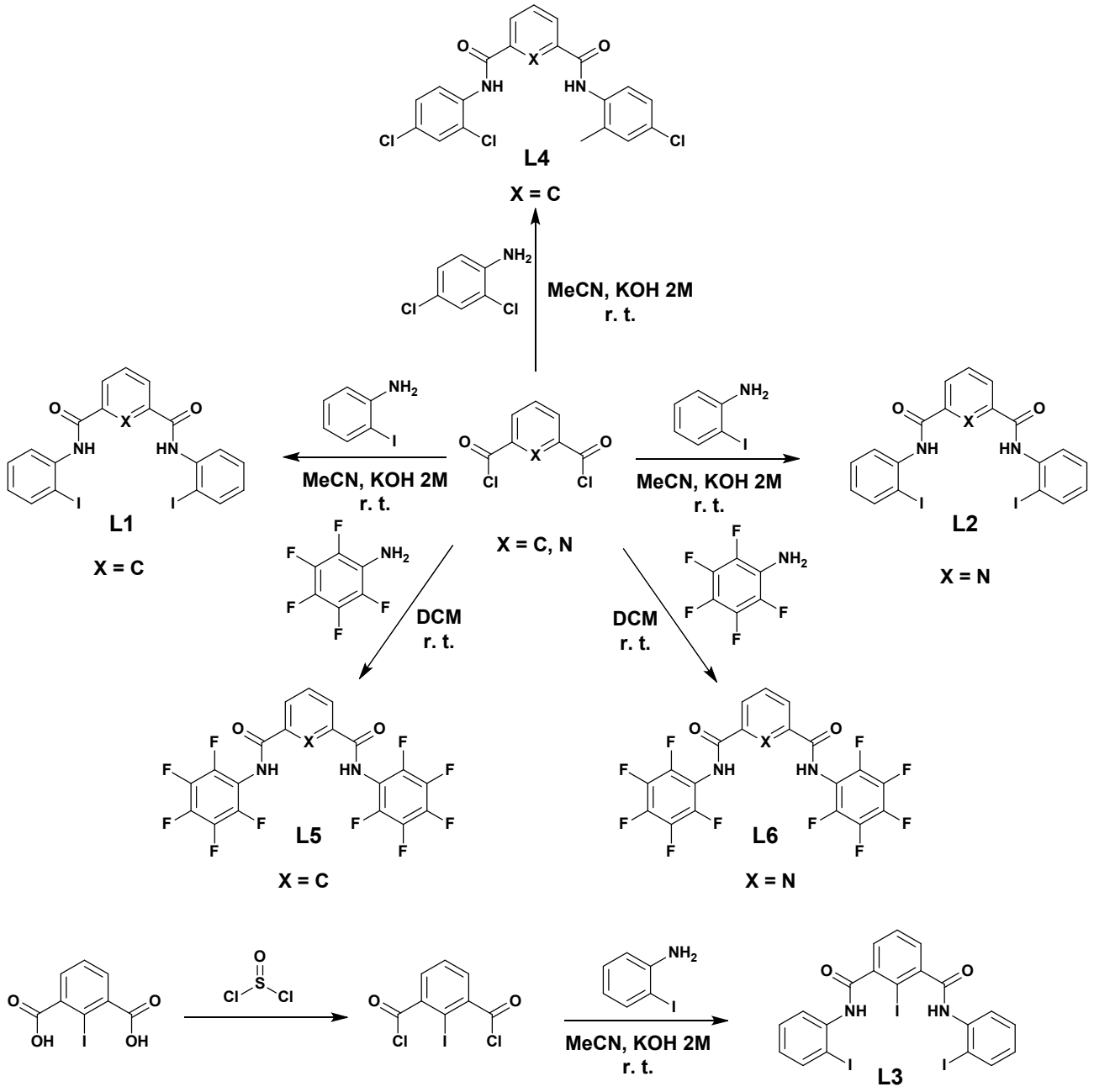

Figure S1 Synthetic schemes for receptors **L1**-**L6**.

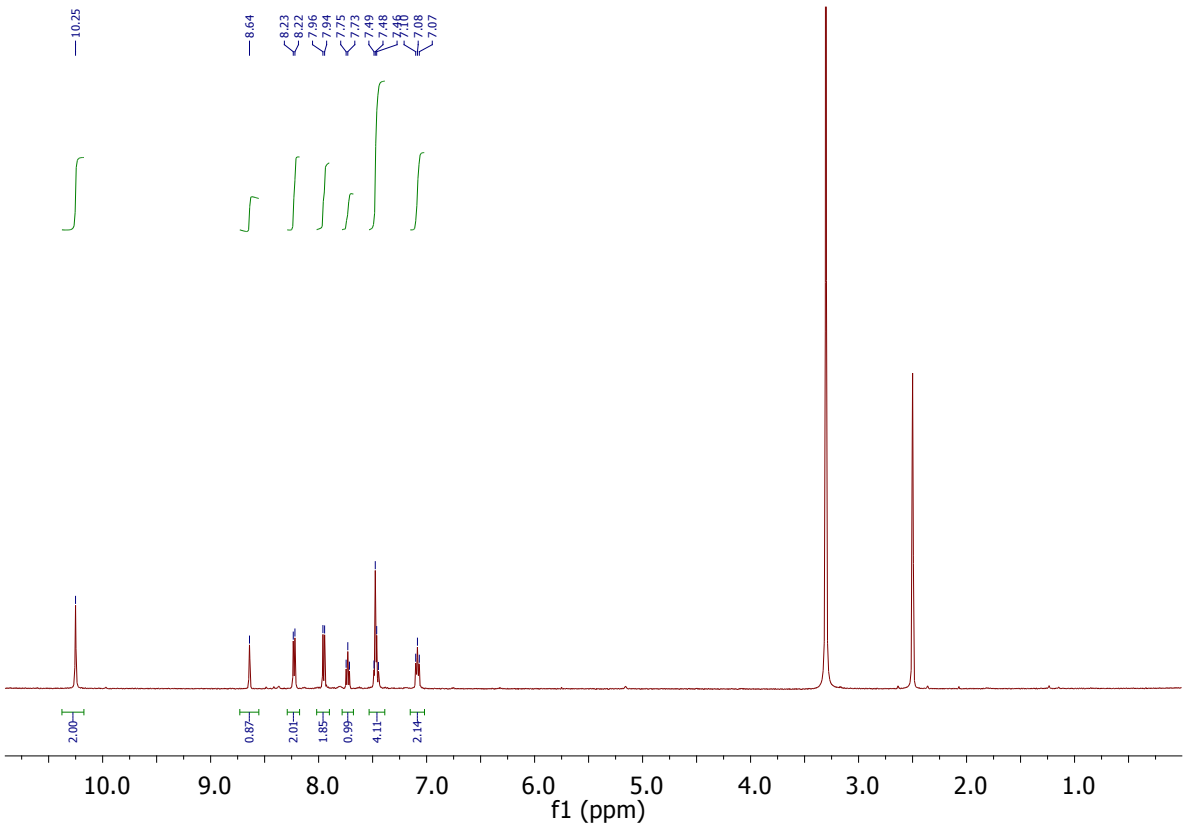

Figure S2 ^{1}H-NMR spectrum of **L1** in DMSO-d_6.

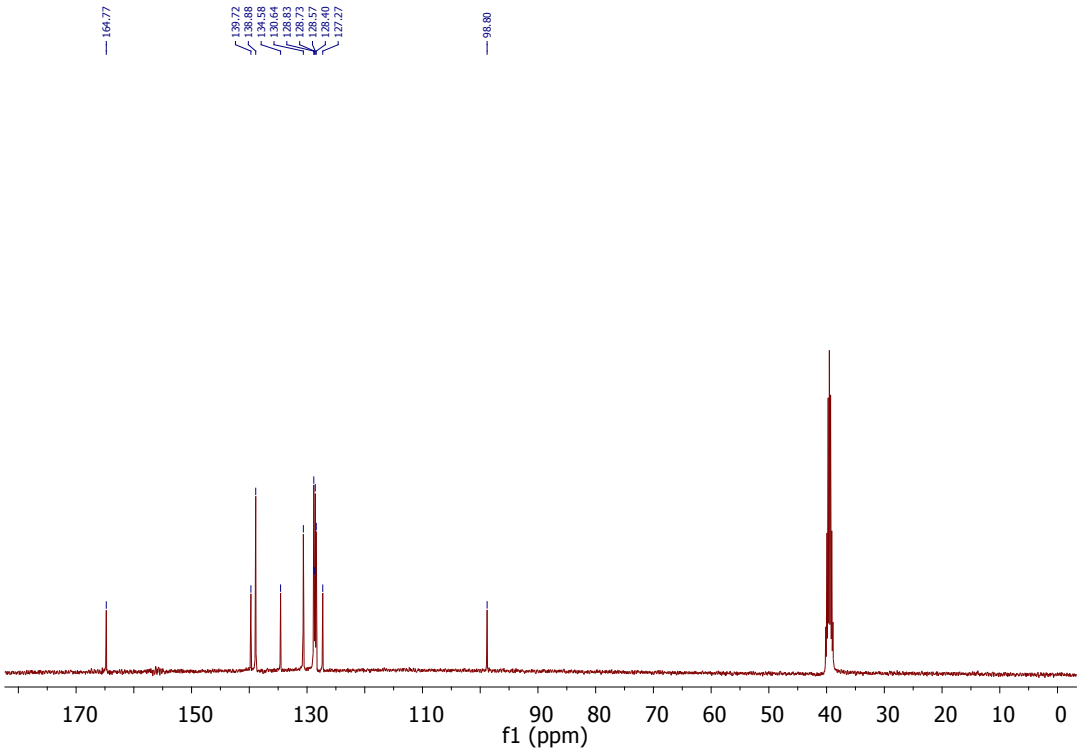

Figure S3 ^{13}C-NMR spectrum of **L1** in DMSO-d_6.

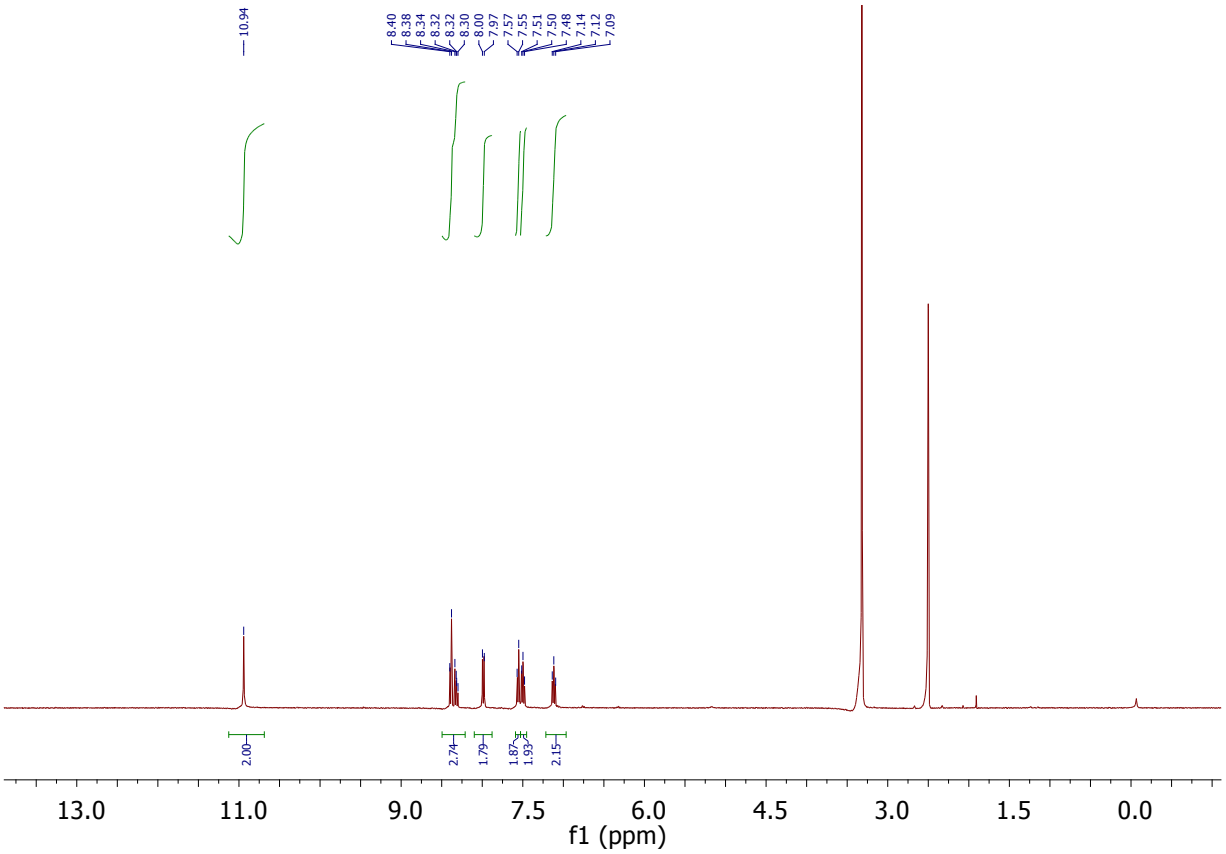

Figure S4 ^{1}H-NMR spectrum of **L2** in DMSO-d_6.

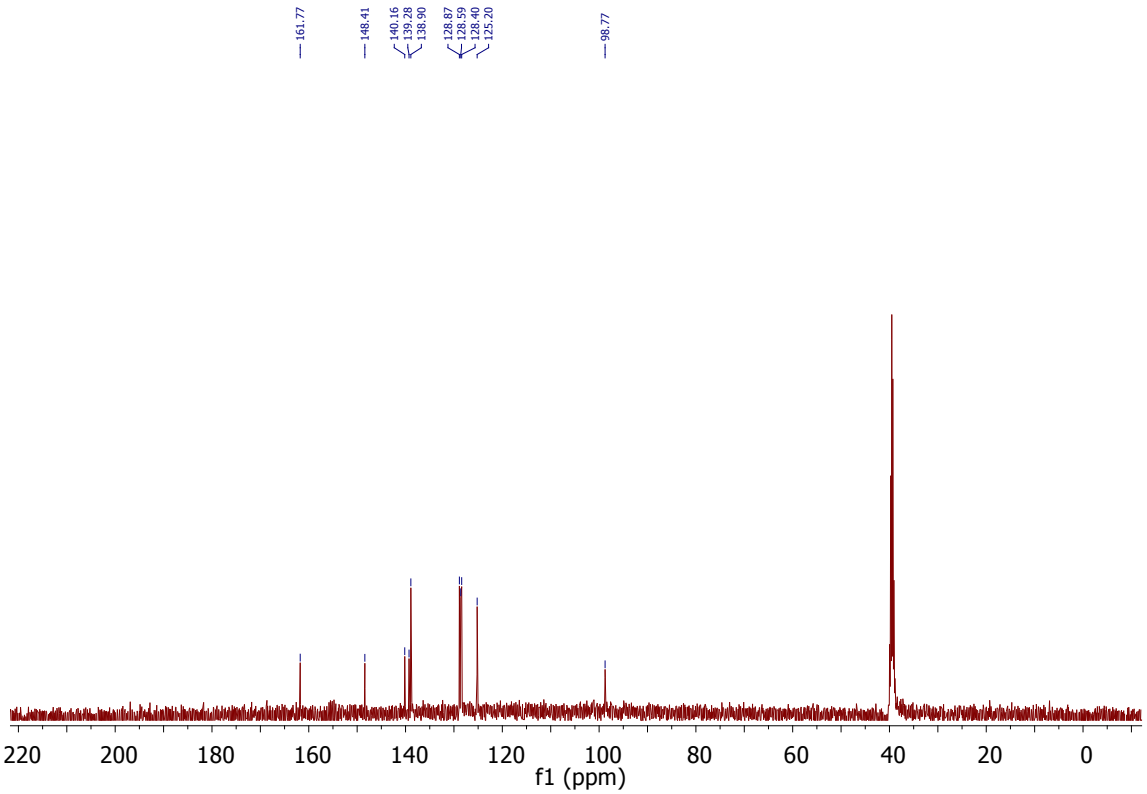

Figure S5 ^{13}C-NMR spectrum of **L2** in DMSO-d_6.

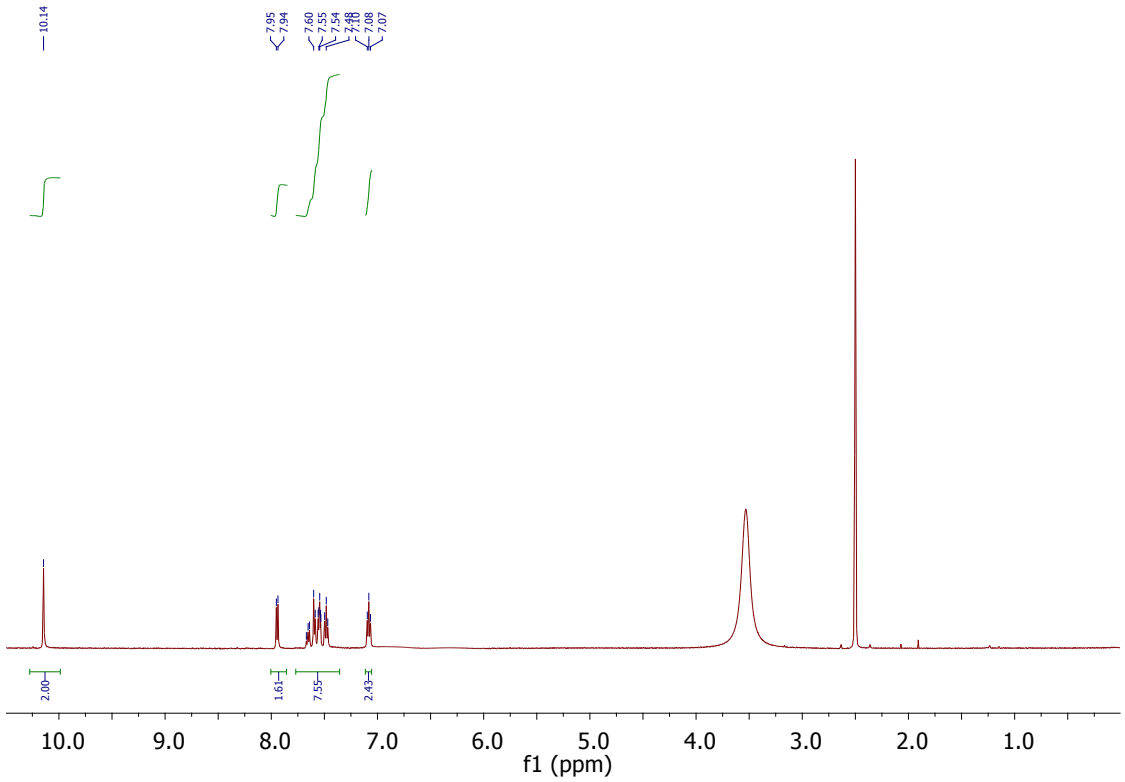

Figure S6 ^{1}H-NMR spectrum of **L3** in DMSO-d_6.

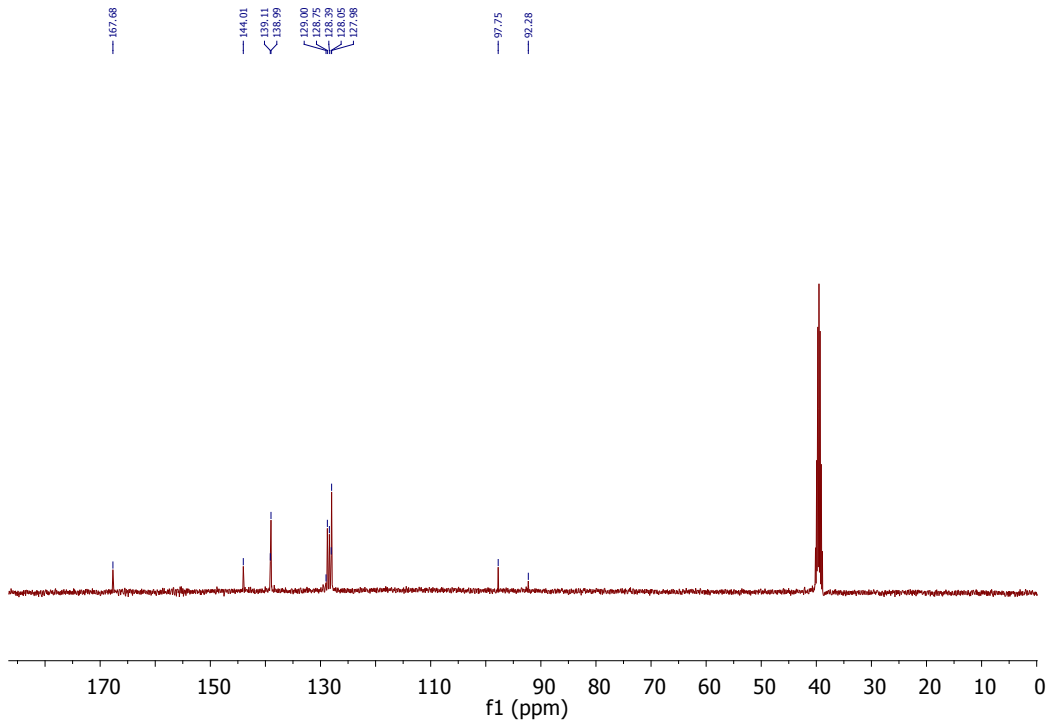

Figure S7 ^{13}C-NMR spectrum of **L3** in DMSO-d_6.

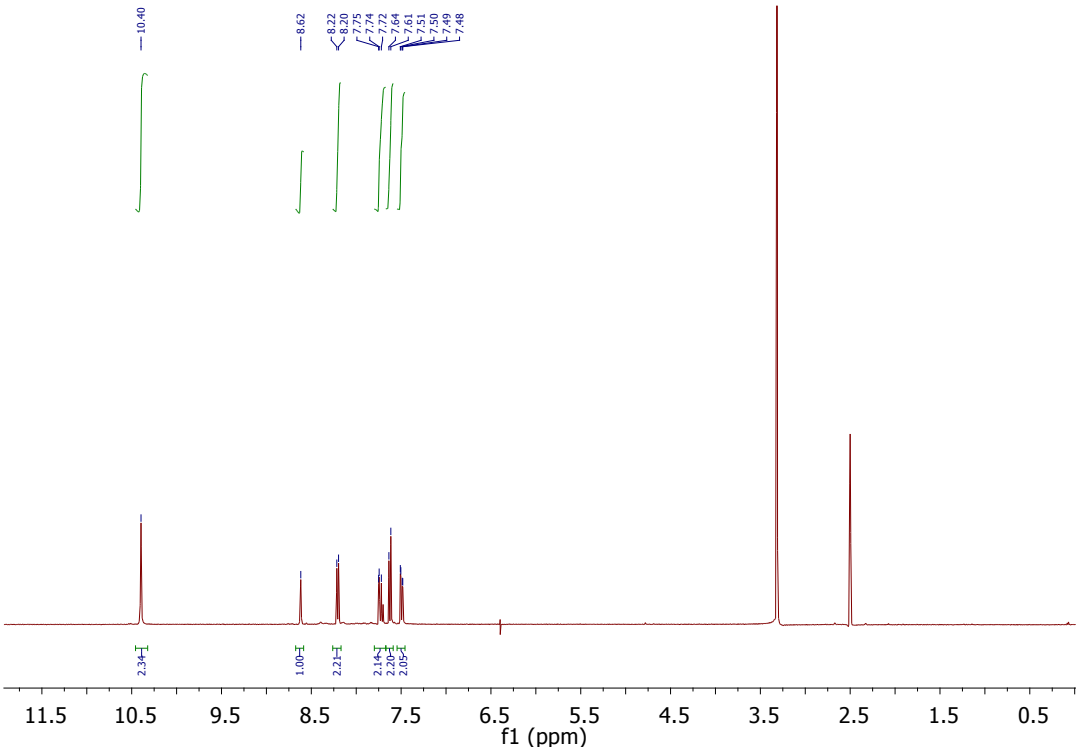

Figure S8 ^{1}H-NMR spectrum of **L4** in DMSO-d_6.

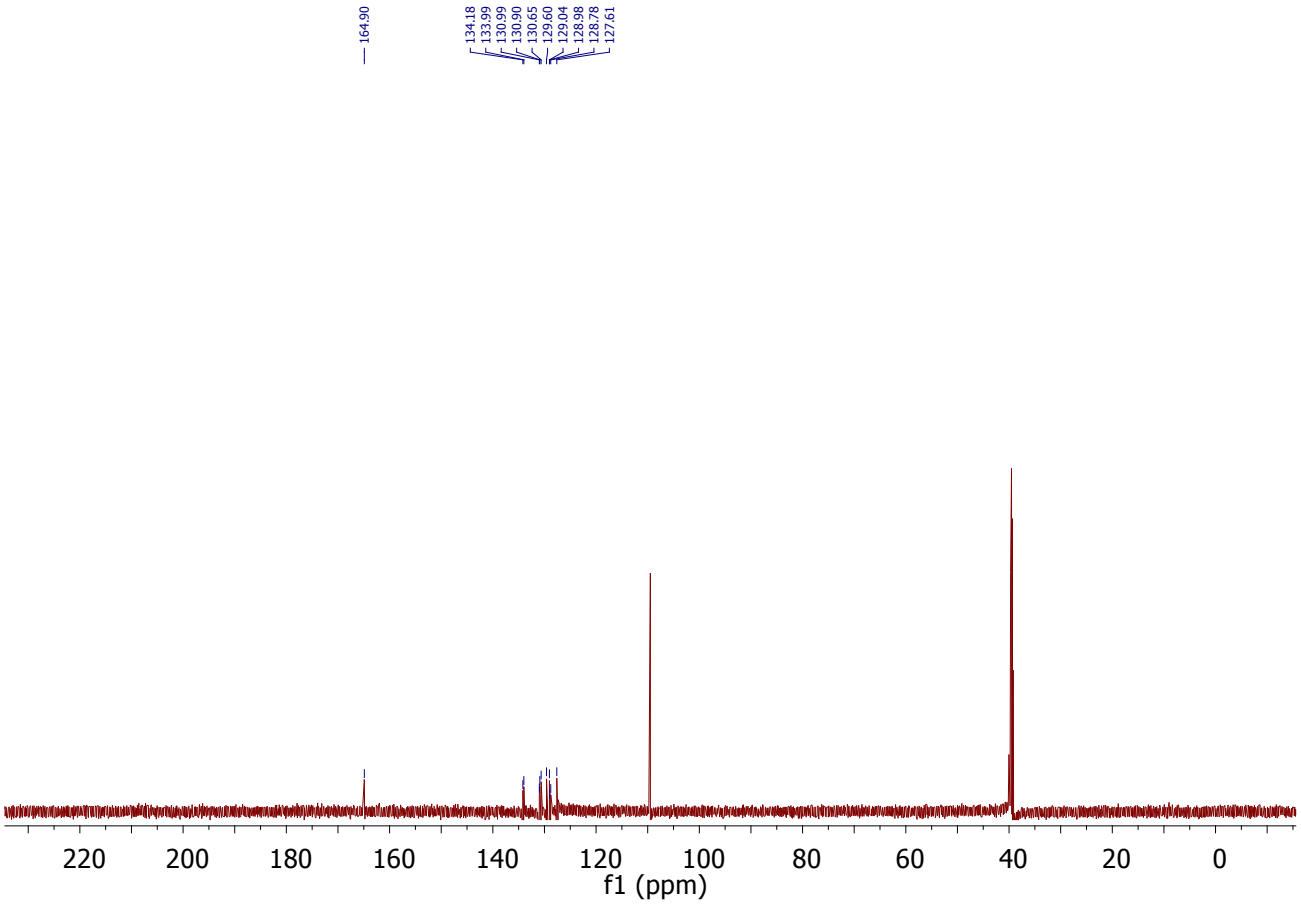

Figure S9 ^{13}C-NMR spectrum of **L4** in DMSO-d_6.

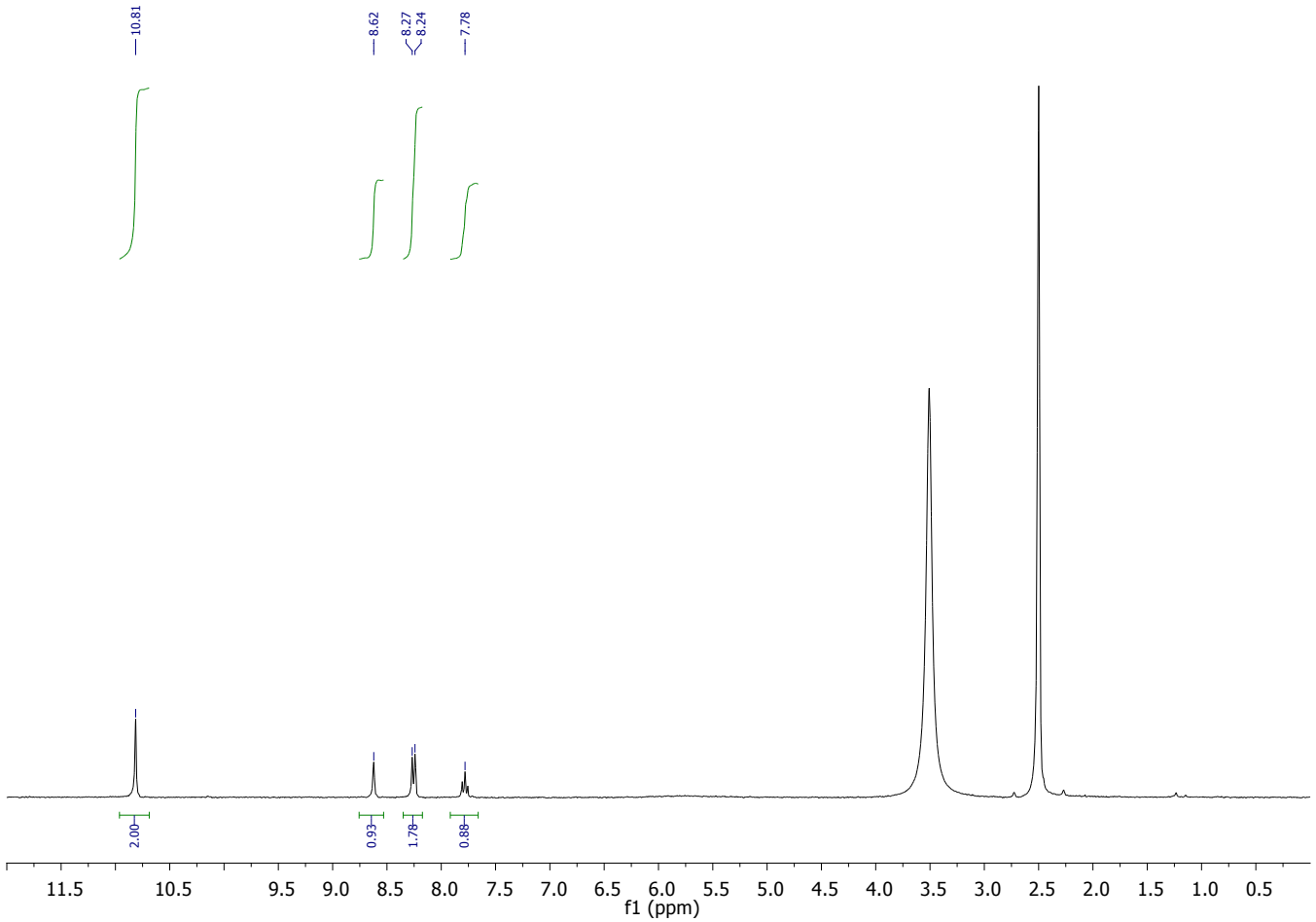

Figure S10 ^{1}H-NMR spectrum of **L5** in DMSO-d_6.

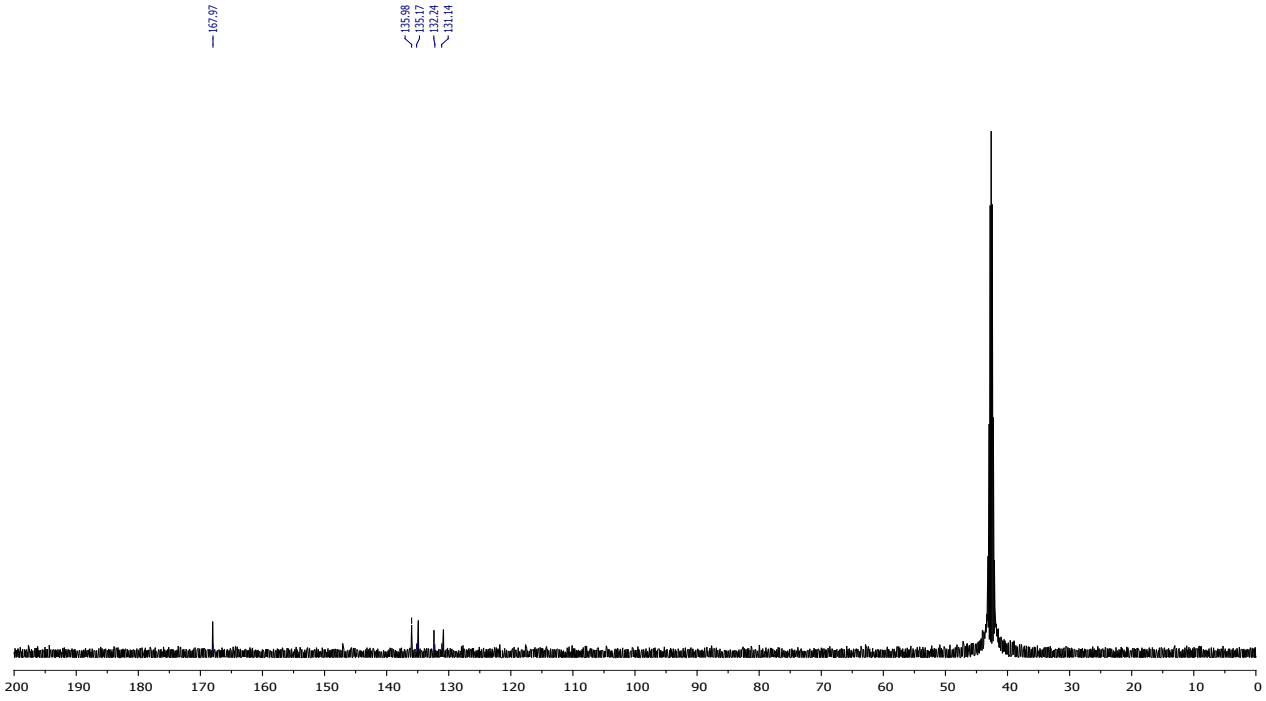

Figure S11 ^{13}C-NMR spectrum of **L5** in DMSO-d_6.

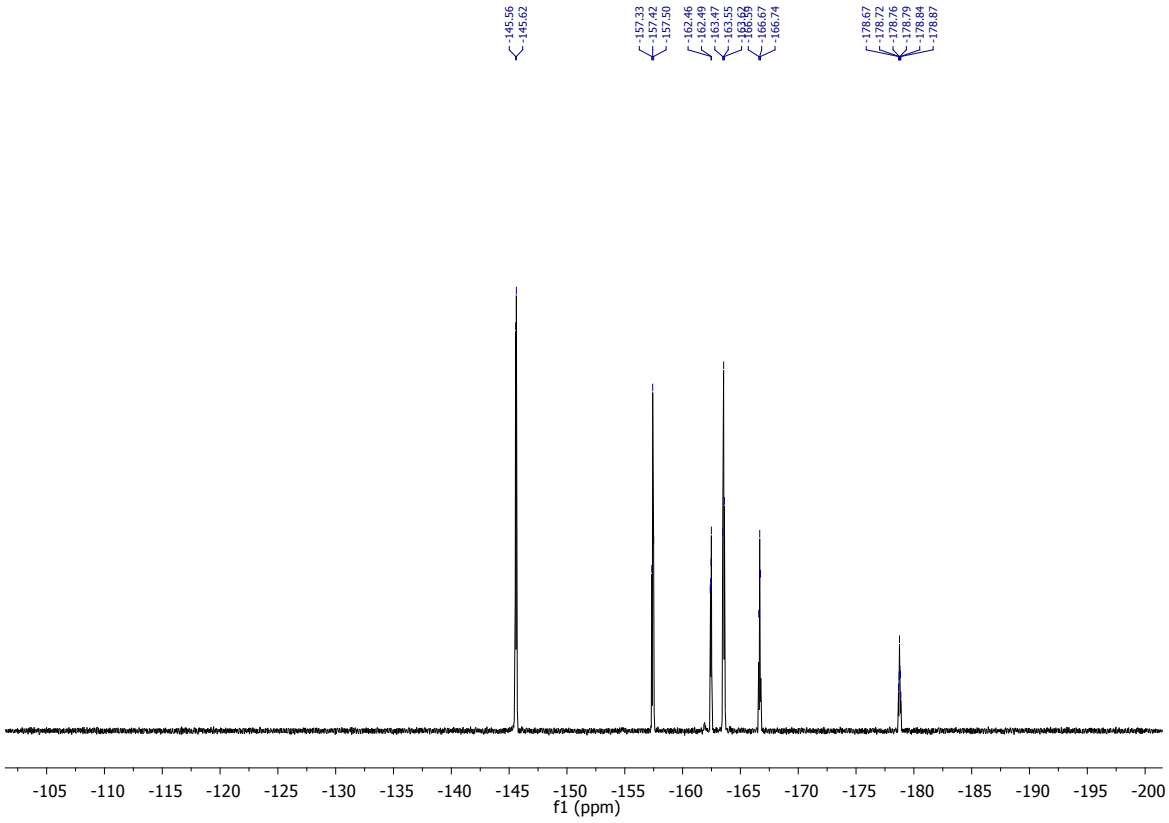

Figure S12 ^{19}F-NMR spectrum of **L5** in DMSO-d_6.

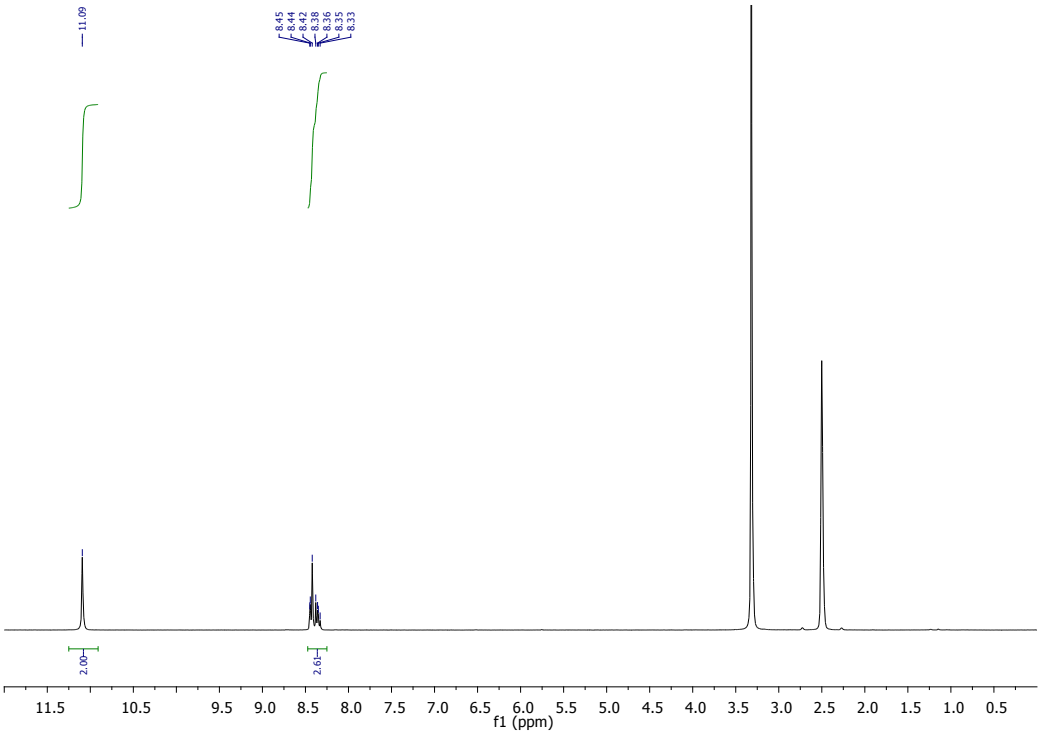

Figure S13 ^{1}H-NMR spectrum of **L6** in DMSO-d_6.

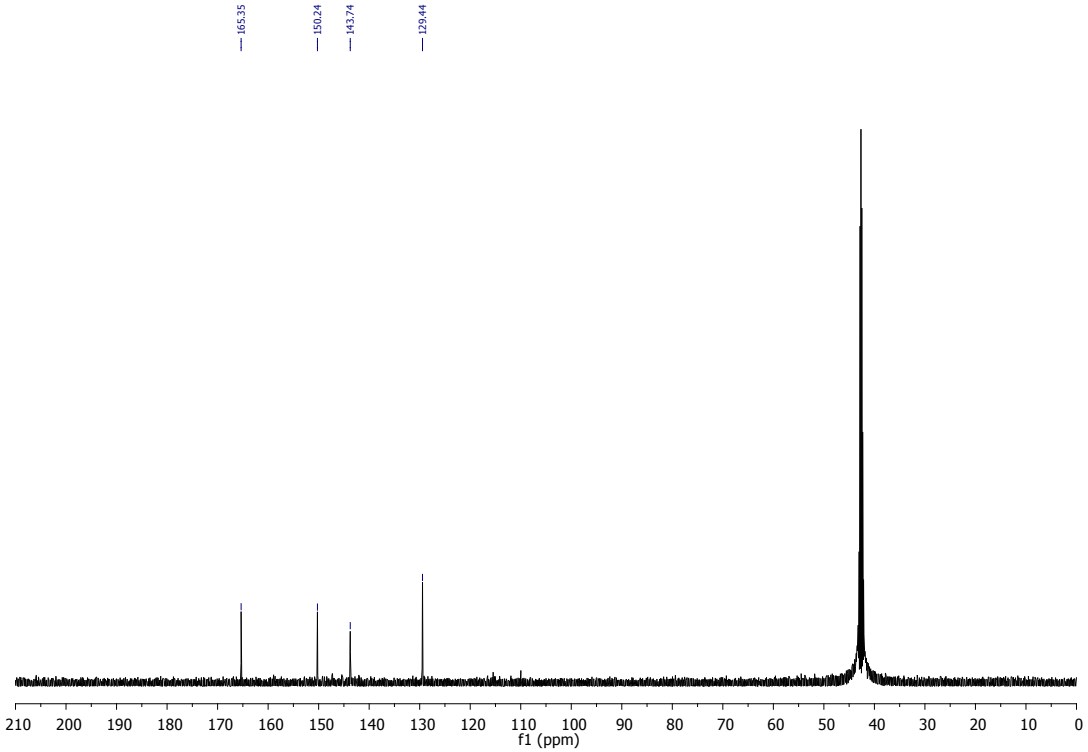

Figure S14 ^{13}C-NMR spectrum of **L6** in DMSO-d_6.

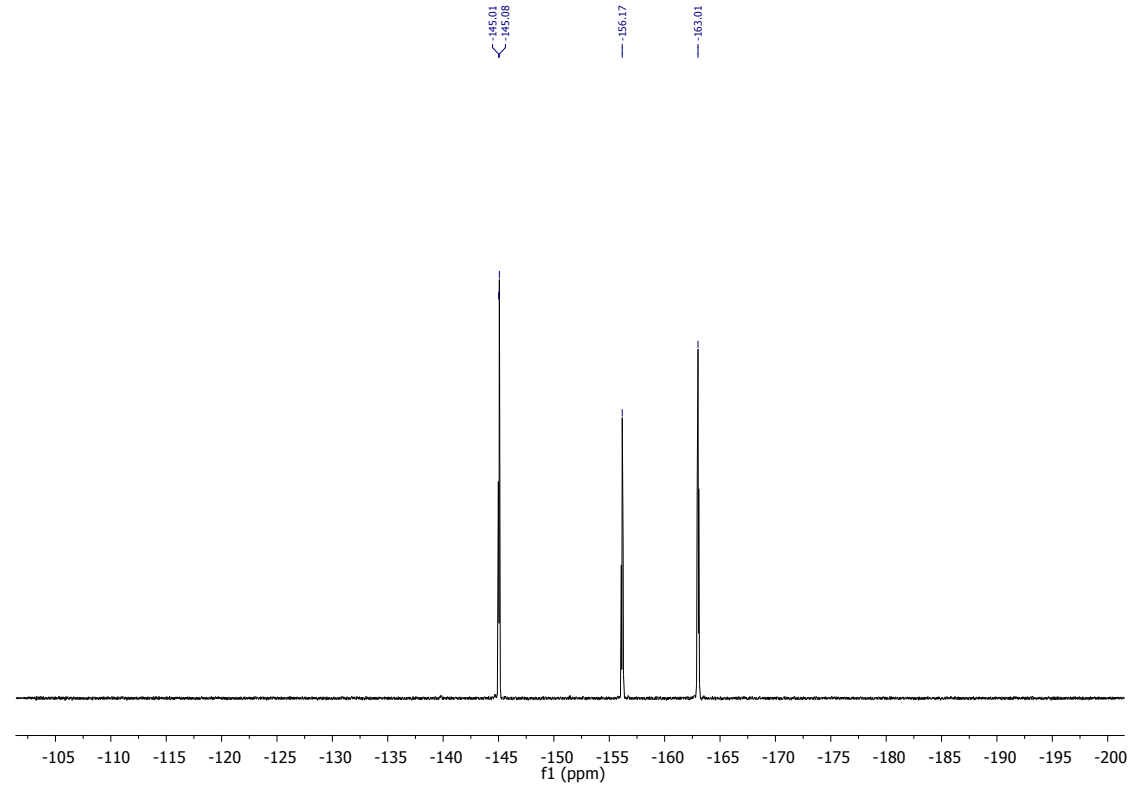

Figure S15 ^{19}F-NMR spectrum of **L6** in DMSO-d_6.

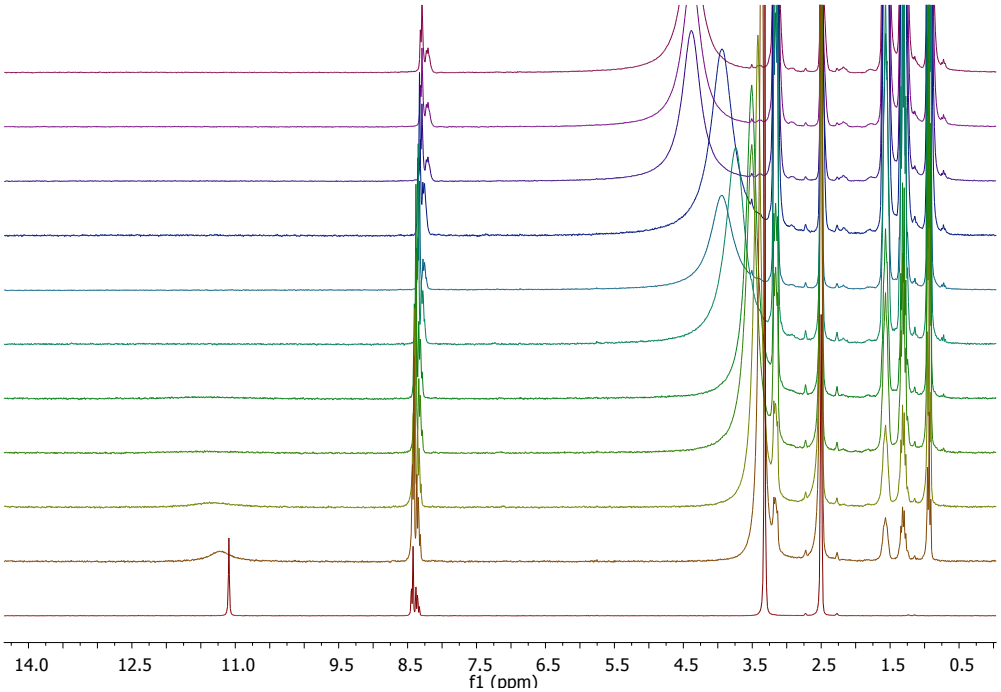

Figure S16 Stack plot of the ^{1}H-NMR spectra of **L6** upon addition of increasing amount of $TBAH_2PO_4$ in DMSO-d_6.

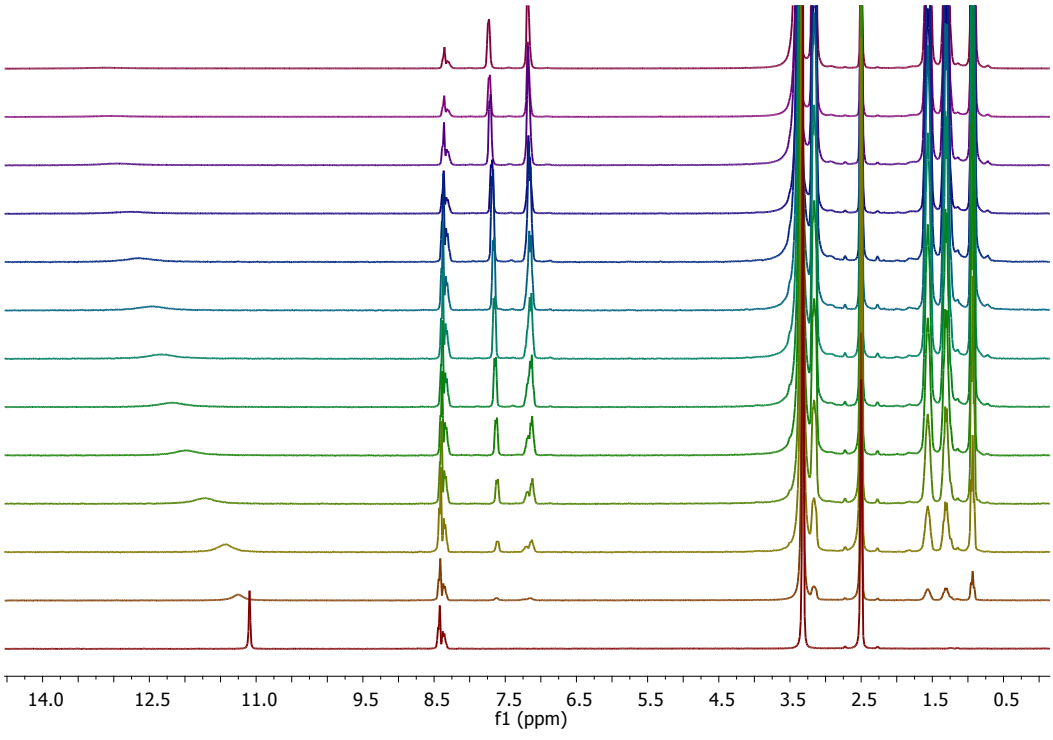

Figure S17 Stack plot of the ^{1}H-NMR spectra of **L6** upon addition of increasing amount of TBABzO in DMSO-d_6.

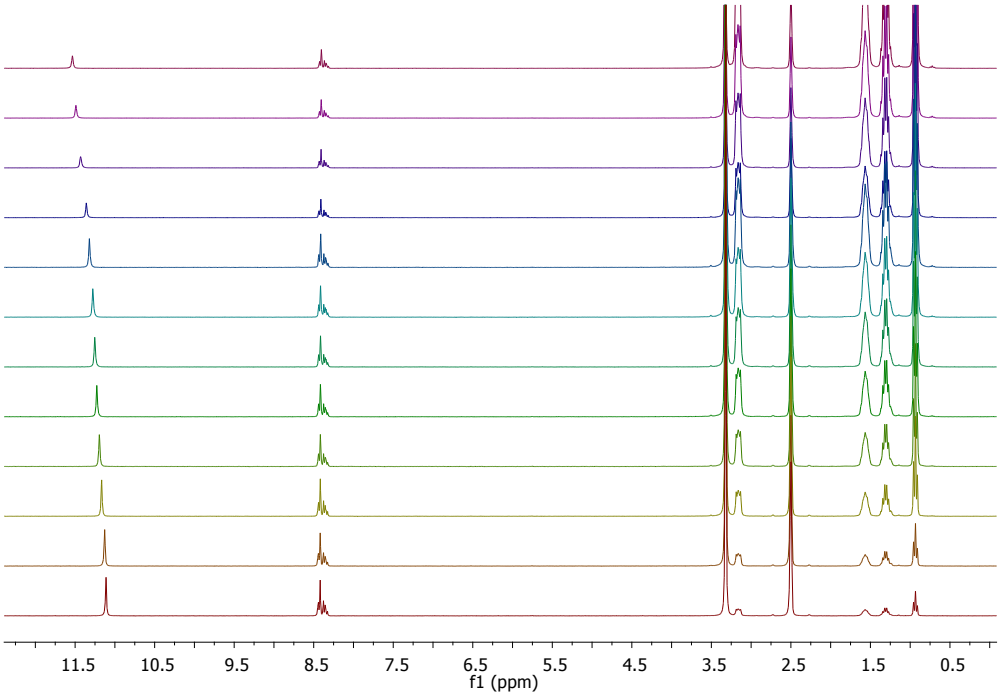

Figure S18 Stack plot of the ^{1}H-NMR spectra of **L6** upon addition of increasing amount of TBACl in DMSO-d_6.

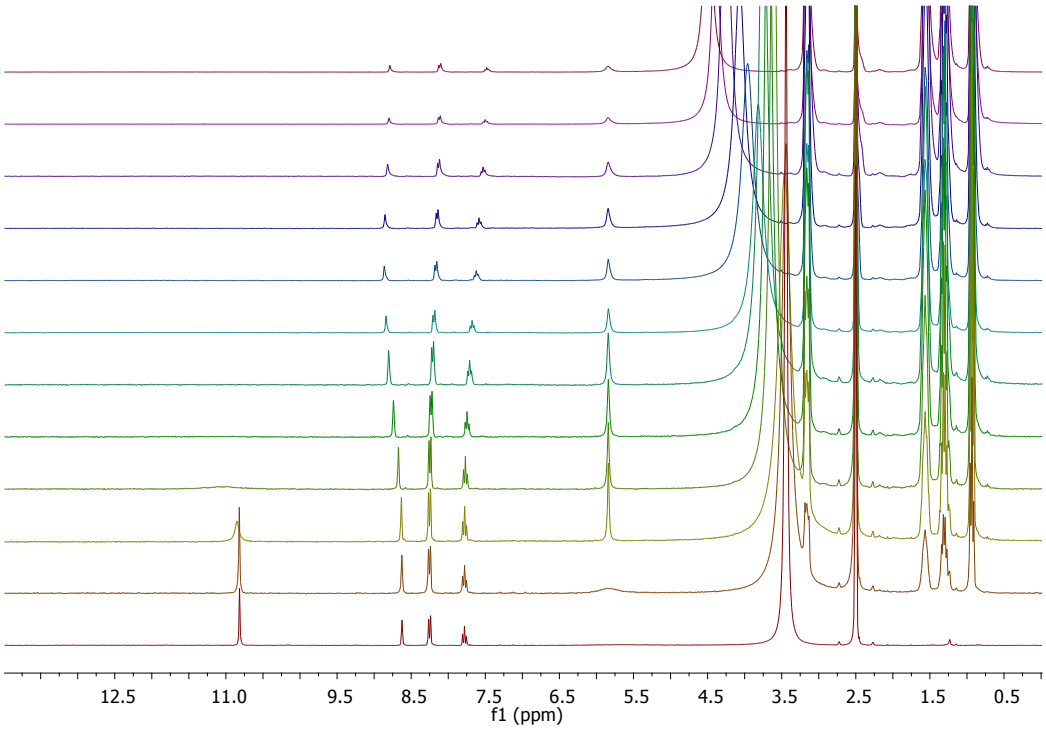

Figure S19 Stack plot of the ^{1}H-NMR spectra of **L5** upon addition of increasing amount of $TBAH_2PO_4$ in DMSO-d_6.

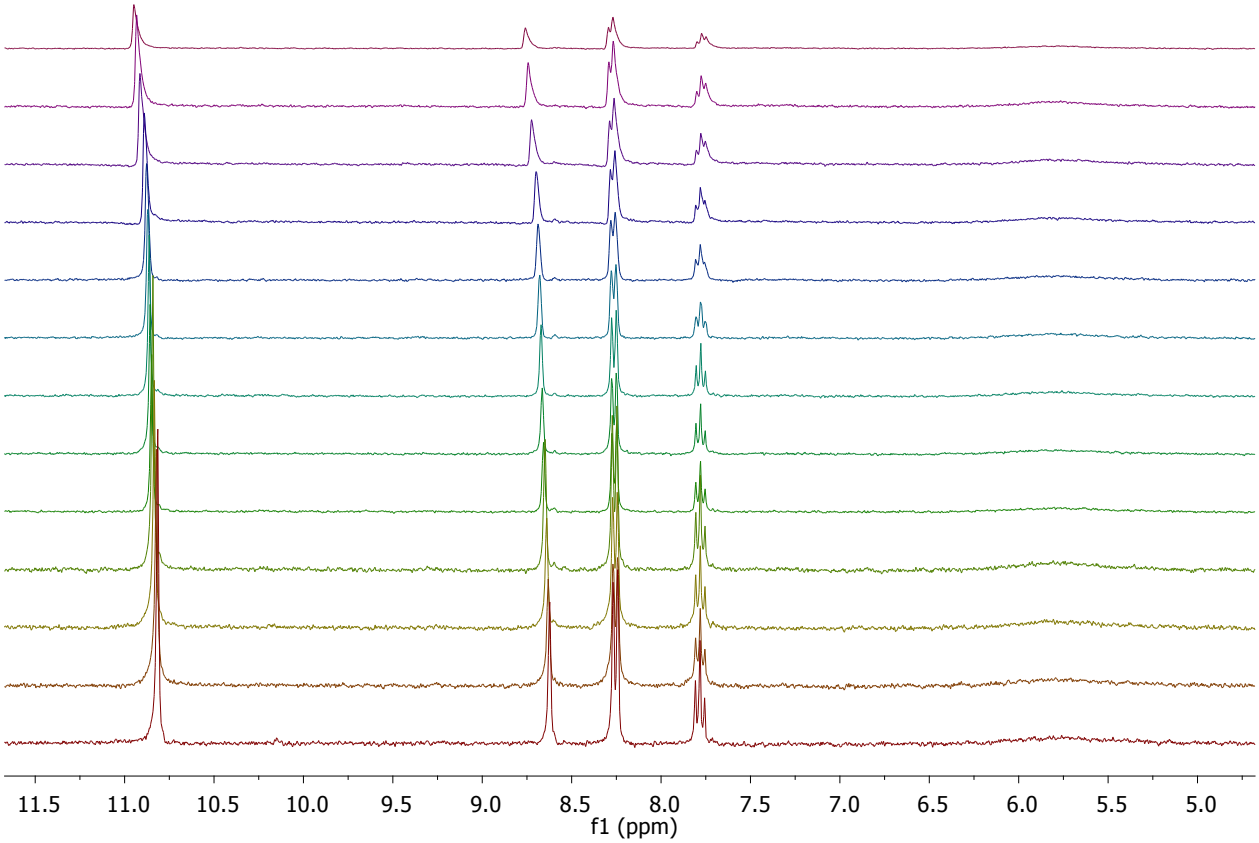

Figure S20 Stack plot of the ^{1}H-NMR spectra of **L5** upon addition of increasing amount of TBACl in DMSO-d_6.

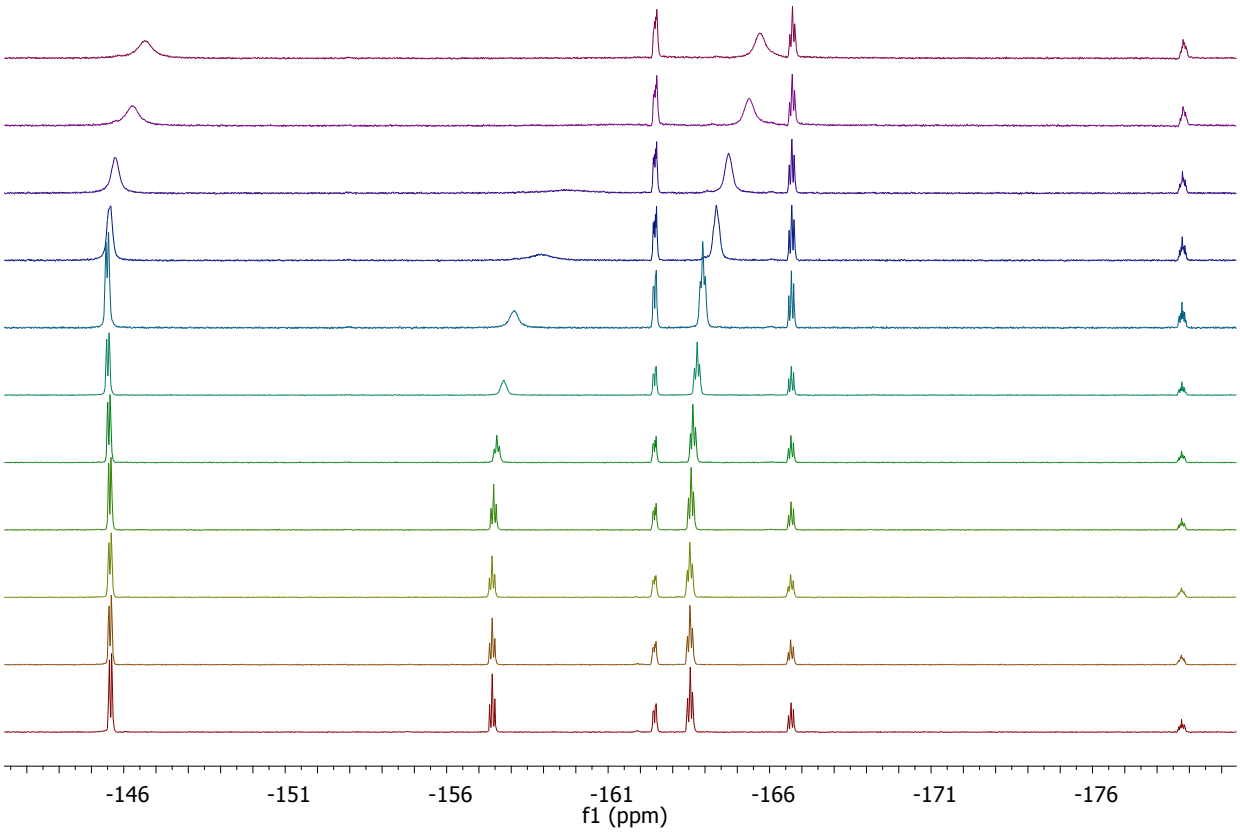

Figure S21 Stack plot of the ^{19}F-NMR spectra of **L5** upon addition of increasing amount of $TBAH_2PO_4$ in DMSO-d_6.

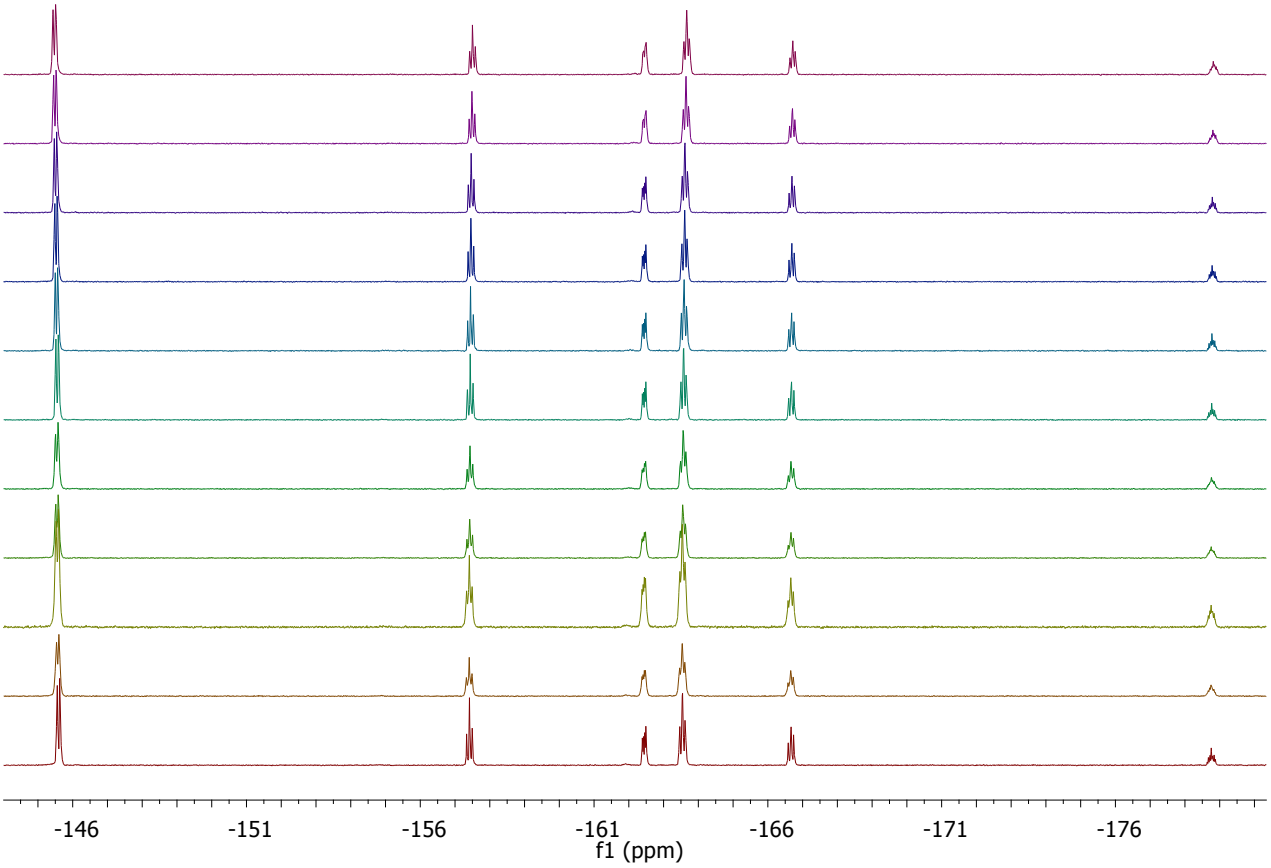

Figure S22 Stack plot of the ^{19}F-NMR spectra of **L5** upon addition of increasing amount of TBACl in DMSO-d_6.

[1]H-NMR fitting

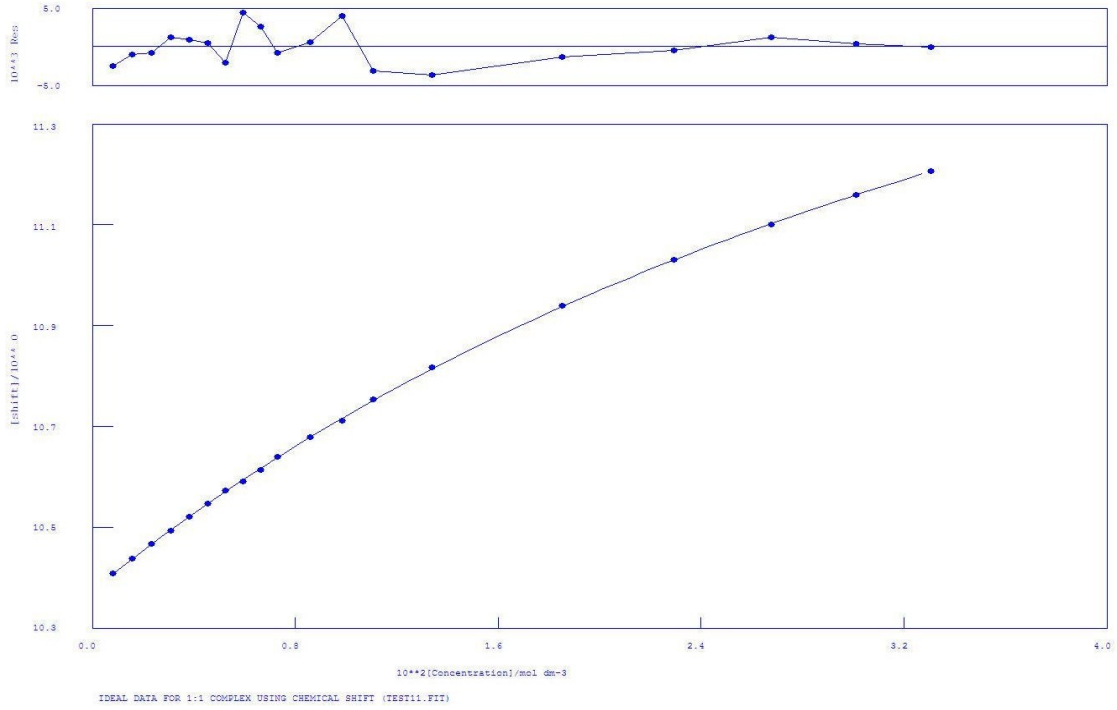

Calculations by WinEQNMR Version 1.20 by Michael J. Hynes

Program run at 18:01:15 on 03/11/2015

IDEAL DATA FOR 1:1 COMPLEX USING CHEMICAL SHIFT (TEST11.FIT)

Reaction: M + L = ML

FILE: TEST11.FIT

IDEAL DATA: K1 = 63.091; DELTA M = 20.0; DELTA ML = 120.0

File prepared by M. J. Hynes, October 22 2000

NO. A PARAMETER DELTA ERROR CONDITION DESCRIPTION

1 1 2.24508E+01 2.000E-01 5.669E-01 1.760E+02 K1

2 1 1.03744E+01 2.000E-01 1.494E-03 5.608E+00 SHIFT M

3 1 1.23976E+01 1.000E+00 3.005E-02 1.416E+02 SHIFT ML

0RMS ERROR = 2.31E-03 MAX ERROR = 4.40E-03 AT OBS.NO. 8

RESIDUALS SQUARED = 8.50E-05

RFACTOR = 0.0197 PERCENT

Figure S23 [1]H-NMR titration of **L4** with TBABzO in DMSO-d_6

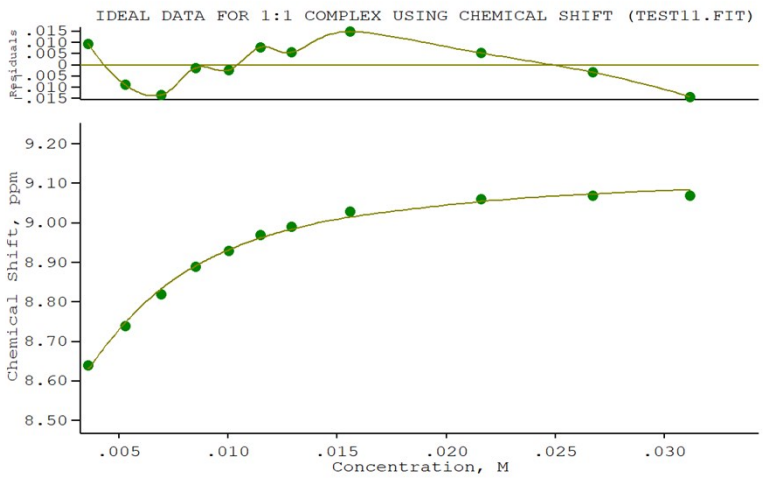

Calculations by WinEQNMR2 Version 2.00 by Michael J. Hynes

Program run at 13:03:17 on 10/09/2018

IDEAL DATA FOR 1:1 COMPLEX USING CHEMICAL SHIFT (TEST11.FIT)

Reaction: Sn + L = Sn(L)

FILE: TEST11.FIT (Measured shift is on 119Sn)

IDEAL DATA: K1 = 63.091; DELTA M = 20.0; DELTA ML = 120.0

File prepared by M. J. Hynes, October 22 2000

Equilibrium constants are floating point numbers

NO.	A	PARAMETER	DELTA	ERROR	CONDITION	DESCRIPTION
1	1	5.36975E+02	2.000E-01	6.586E+01	1.937E+01	K1
2	1	8.26540E+00	2.000E-01	2.907E-02	6.824E+00	SHIFT Sn
3	1	9.14158E+00	1.000E+00	1.182E-02	8.037E+00	SHIFT Sn(L)

0RMS ERROR = 1.07E-02 MAX ERROR = 1.49E-02 AT OBS.NO. 8

RESIDUALS SQUARED = 9.11E-04

RFACTOR = 0.1019 PERCENT

Figure S24 ^{1}H-NMR titration of **L5** with TBABzO in DMSO-d_6

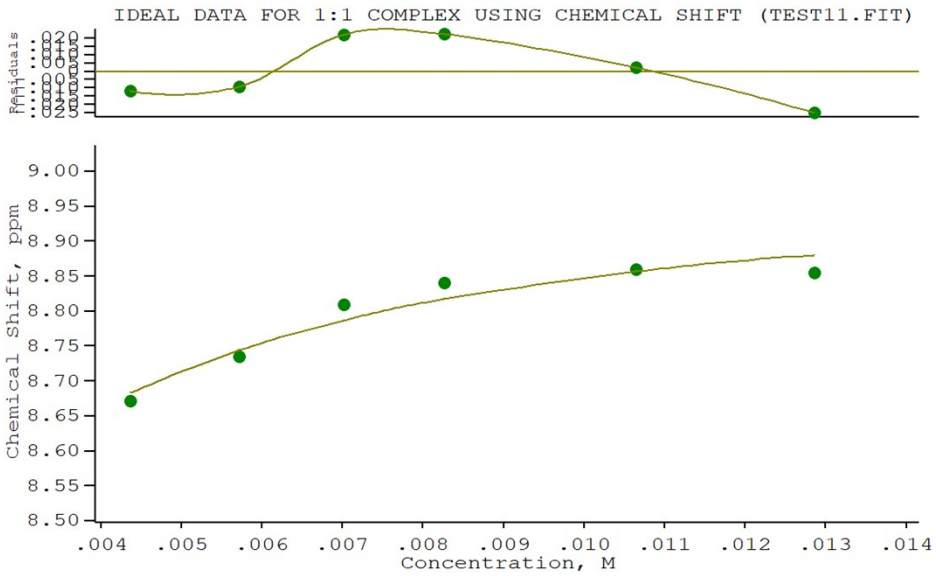

Calculations by WinEQNMR2 Version 2.00 by Michael J. Hynes

Program run at 17:33:25 on 11/22/2018

IDEAL DATA FOR 1:1 COMPLEX USING CHEMICAL SHIFT (TEST11.FIT)

Reaction: Sn + L = Sn(L)

FILE: TEST11.FIT (Measured shift is on 119Sn)

IDEAL DATA: K1 = 63.091; DELTA M = 20.0; DELTA ML = 120.0

File prepared by M. J. Hynes, October 22 2000

Equilibrium constants are floating point numbers

NO.	A	PARAMETER	DELTA	ERROR	CONDITION	DESCRIPTION
1	1	6.38163E+02	2.000E-01	1.373E+02	3.048E+00	K1
2	1	8.36498E+00	2.000E-01	6.839E-02	4.443E+00	SHIFT Sn
3	1	8.97297E+00	1.000E+00	3.254E-02	5.213E+00	SHIFT Sn(L)

0RMS ERROR = 2.49E-02 MAX ERROR = 2.51E-02 AT OBS.NO. 6

RESIDUALS SQUARED = 1.87E-03

RFACTOR = 0.2005 PERCENT

Figure S25 ^{1}H-NMR titration of **L5** with $TBAH_2PO_4$ in DMSO-d_6

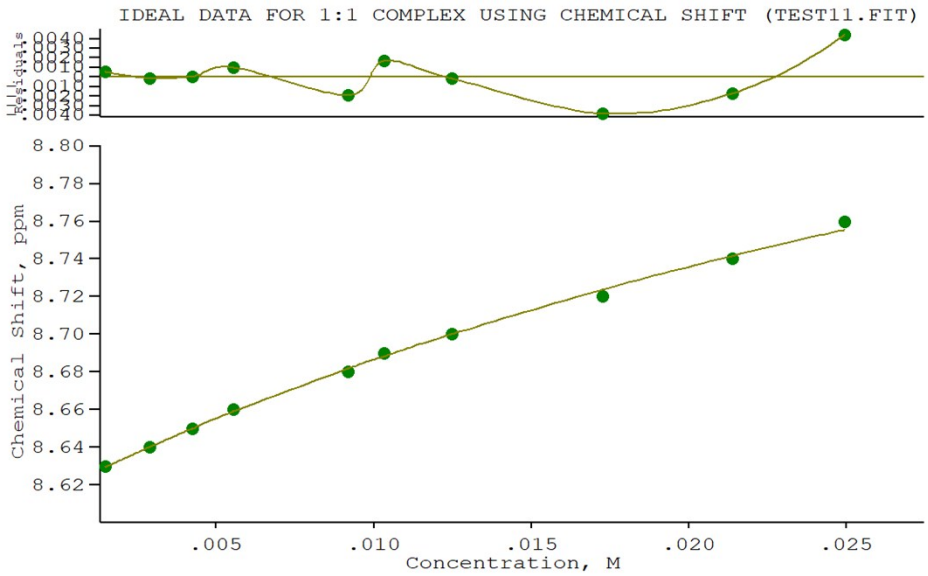

Calculations by WinEQNMR2 Version 2.00 by Michael J. Hynes

Program run at 13:20:36 on 10/09/2018

IDEAL DATA FOR 1:1 COMPLEX USING CHEMICAL SHIFT (TEST11.FIT)

Reaction: Sn + L = Sn(L)

FILE: TEST11.FIT (Measured shift is on 119Sn)

IDEAL DATA: K1 = 63.091; DELTA M = 20.0; DELTA ML = 120.0

File prepared by M. J. Hynes, October 22 2000

Equilibrium constants are floating point numbers

NO. A PARAMETER DELTA ERROR CONDITION DESCRIPTION

1 1 2.20801E+01 2.000E-01 4.468E+00 1.923E+02 K1

2 1 8.61786E+00 2.000E-01 2.233E-03 5.464E+00 SHIFT Sn

3 1 9.02173E+00 1.000E+00 5.088E-02 1.582E+02 SHIFT Sn(L)

0RMS ERROR = 2.53E-03 MAX ERROR = 4.44E-03 AT OBS.NO. 10

RESIDUALS SQUARED = 4.47E-05

RFACTOR = 0.0243 PERCENT

Figure S26 ^{1}H-NMR titration of **L5** with TBACl in DMSO-d_6

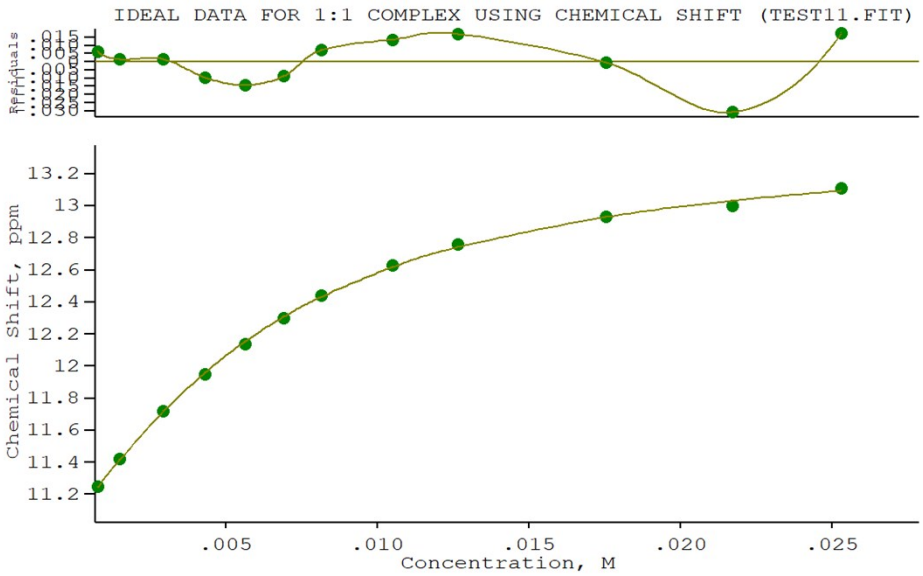

Calculations by WinEQNMR2 Version 2.00 by Michael J. Hynes

Program run at 15:45:01 on 11/22/2018

IDEAL DATA FOR 1:1 COMPLEX USING CHEMICAL SHIFT (TEST11.FIT)

Reaction: Sn + L = Sn(L)

FILE: TEST11.FIT (Measured shift is on 119Sn)

IDEAL DATA: K1 = 63.091; DELTA M = 20.0; DELTA ML = 120.0

File prepared by M. J. Hynes, October 22 2000

Equilibrium constants are floating point numbers

NO.	A	PARAMETER	DELTA	ERROR	CONDITION	DESCRIPTION
1	1	2.58384E+02	2.000E-01	1.257E+01	1.636E+01	K1
2	1	1.10516E+01	2.000E-01	1.377E-02	2.753E+00	SHIFT Sn
3	1	1.34692E+01	1.000E+00	2.669E-02	1.163E+01	SHIFT Sn(L)

0RMS ERROR = 1.55E-02 MAX ERROR = 3.06E-02 AT OBS.NO. 11

RESIDUALS SQUARED = 2.18E-03

RFACTOR = 0.1093 PERCENT

Figure S27 ^{1}H-NMR titration of **L6** with TBABzO in DMSO-d_6

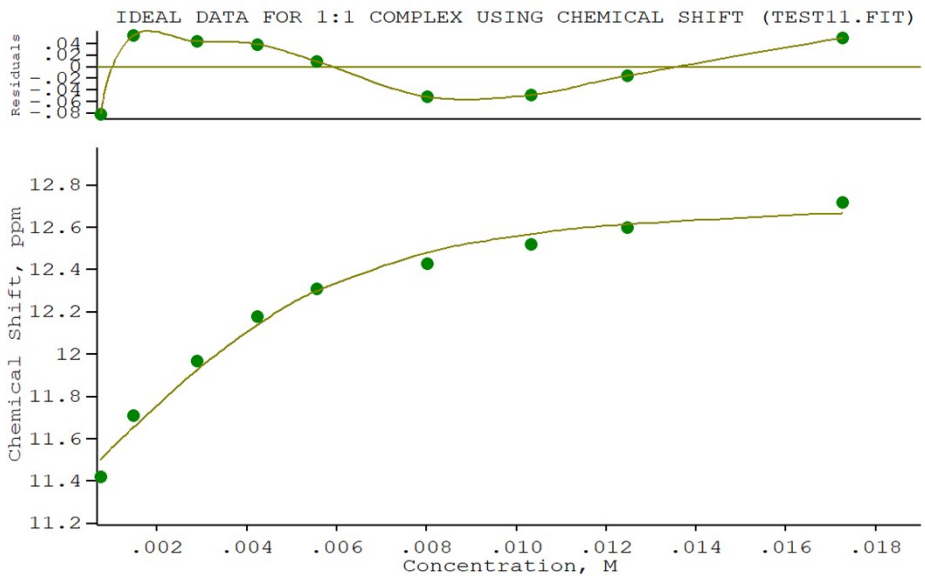

Calculations by WinEQNMR2 Version 2.00 by Michael J. Hynes

Program run at 17:54:00 on 11/22/2018

IDEAL DATA FOR 1:1 COMPLEX USING CHEMICAL SHIFT (TEST11.FIT)

Reaction: Sn + L = Sn(L)

FILE: TEST11.FIT (Measured shift is on 119Sn)

IDEAL DATA: K1 = 63.091; DELTA M = 20.0; DELTA ML = 120.0

File prepared by M. J. Hynes, October 22 2000

Equilibrium constants are floating point numbers

NO. A PARAMETER DELTA ERROR CONDITION DESCRIPTION

1 1 1.07465E+03 2.000E-01 2.166E+02 3.611E+00 K1

2 1 1.13394E+01 2.000E-01 4.960E-02 1.479E+00 SHIFT Sn

3 1 1.27692E+01 1.000E+00 5.336E-02 3.224E+00 SHIFT Sn(L)

0RMS ERROR = 5.95E-02 MAX ERROR = 8.24E-02 AT OBS.NO. 1

RESIDUALS SQUARED = 2.12E-02

RFACTOR = 0.3976 PERCENT

Figure S28 ^{1}H-NMR titration of **L6** with $TBAH_2PO_4$ in DMSO-d_6

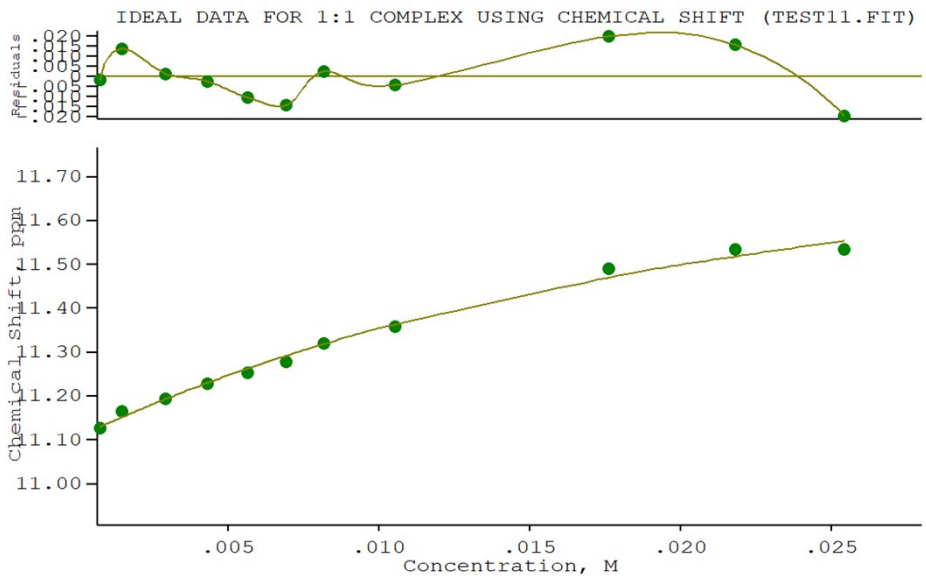

Calculations by WinEQNMR2 Version 2.00 by Michael J. Hynes

Program run at 16:05:59 on 11/22/2018

IDEAL DATA FOR 1:1 COMPLEX USING CHEMICAL SHIFT (TEST11.FIT)

Reaction: Sn + L = Sn(L)

FILE: TEST11.FIT (Measured shift is on 119Sn)

IDEAL DATA: K1 = 63.091; DELTA M = 20.0; DELTA ML = 120.0

File prepared by M. J. Hynes, October 22 2000

Equilibrium constants are floating point numbers

NO. A PARAMETER DELTA ERROR CONDITION DESCRIPTION

1 1 4.68057E+01 2.000E-01 1.151E+01 6.088E+01 K1

2 1 1.11055E+01 2.000E-01 1.124E-02 4.233E+00 SHIFT Sn

3 1 1.19704E+01 1.000E+00 9.705E-02 4.566E+01 SHIFT Sn(L)

0RMS ERROR = 1.40E-02 MAX ERROR = 2.00E-02 AT OBS.NO. 9

RESIDUALS SQUARED = 1.56E-03

RFACTOR = 0.1053 PERCENT

Figure S29 ^{1}H-NMR titration of **L6** with TBACl in DMSO-d_6

Metadynamic simulations

The ligands were fully quantum-mechanically minimized at the DFT/B3LYP level of theory LACVP* basis set with Jaguar.[1] Each binary system was solvated in an orthorhombic box using DMSO molecules, extended 50 Å away from any ligands atom. The dynamics simulation was performed with Desmond[2] and included a starting relaxation step followed by a final metadynamics production phase of 20 ns. In particular, the relaxation step comprised the following: (a) a stage of 100 ps at 10 K retaining the harmonic restraints on the solute heavy atoms (force constant of 50.0 kcal mol^{-1} $Å^{-2}$) using the NPT ensemble with Brownian dynamics; (b) a stage of 12 ps at 10 K with harmonic restraints on the solute heavy atoms (force constant of 50.0 kcal mol^{-1} $Å^{-2}$), using the NVT ensemble and Berendsen thermostat; (c) a stage of 12 ps at 10 K and 1 atm, retaining the harmonic restraints and using the NPT ensemble and Berendsen thermostat and barostat; (f) a stage of 12 ps at 300 K and 1 atm, retaining the harmonic restraints and using the NPT ensemble and Berendsen thermostat and barostat; (g) a final 24 ps stage at 300 K and 1 atm without harmonic restraints, using the NPT Berendsen thermostat and barostat.

Metadynamics (MtD) progressively builds up a history dependent Gaussian-shaped biasing potential long specifically designed descriptors of the model, which are known as collective variables (CVs). MtD simulation was used to disable the ligands to depart each other.

The Gaussian potential is used as:

$$V(s,t) = \sum_{t_i} H \exp\left(-\frac{|s - s(t_i)|^2}{2w^2}\right)$$

Herein, 'H' is the height of the hill, 'w' is the width, 't' is time and 's' is the CV. In MtD the bias or hills are dynamically placed on the top potential energy landscape, which discourages the system to return back to the previous point at a time interval of dt. Center-of-mass (COM) separation between the ligand molecules was considered as a CV. MtD has been performed in the NVT-ensemble at temperature 300 K with Gaussian hills height = 0.03 kJ mol^{-1}, width = 0.05 Å and wall = 10 Å. The atomic coordinates of the system were saved every 50 ps along the MD trajectory. The free energy surface (FES) diagram according to the values of the CV was generated with the Desmond MtD analysis tool.

PCA analysis was performed using Simca[3]. Conformers were described by distances and angles defined in Table S1 and Scheme S1

References

1. Schrödinger Release 2019-2: Jaguar, New York, NY, 2019, v.10.3.

2. Schrödinger Release 2019-2: Desmond Molecular Dynamics System, D. E. Shaw Research, New York, NY, 2019, v.5.7.

3. . SIMCA-P 8.0, Umetrics.

***L5/$H_2PO_4^-$ adduct*.**

The first two principal components (PCs) account for the 50% of the overall variance (Fig S30). Cluster 1 (grey points) refers to frames where **L5** and $H_2PO_4^-$ are not in H bond distance; in cluster 2, the magenta points represent conformations where only a H-bond between $H_2PO_4^-$ and one amidic nitrogen of **L5** occurs (Fig S31a), while in the conformers represented by the light pink points an additional H-bond involves a phosphate oxygens donor and a ligand carbonyl oxygen as acceptor (Fig S17b). Cluster 3 (red and brown points) receives conformations characterized by the formation of two H-bonds, involving both the amidic nitrogens as donor atoms (Fig S31 c,d).

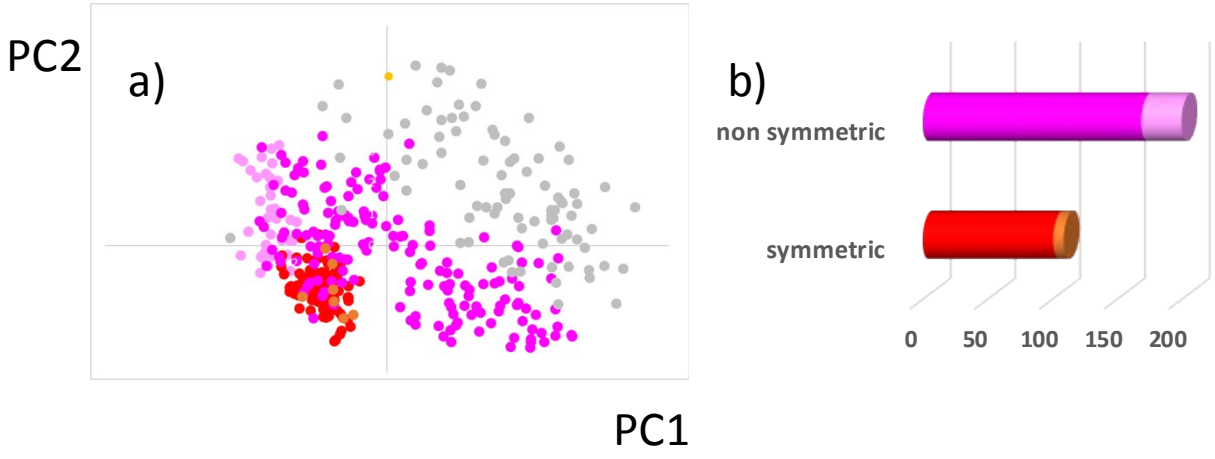

(a) (b)

Figure S30– ***L5/$H_2PO_4^-$ adduct*** - Results from PCA analysis of frames from metadynamic trajectory: (a) PC1 vs PC2 score plot; (b) counting of the symmetric and asymmetric frames classified on the basis of the ligand/substrate H-bonds. (magenta: 1 H-bond involving the amidic nitrogen; light pink: 1 H-bond involving the amidic nitrogen and 1 H-bond involving the carbonyl oxygen; red and brown: 2 H-bond; grey: no interaction)

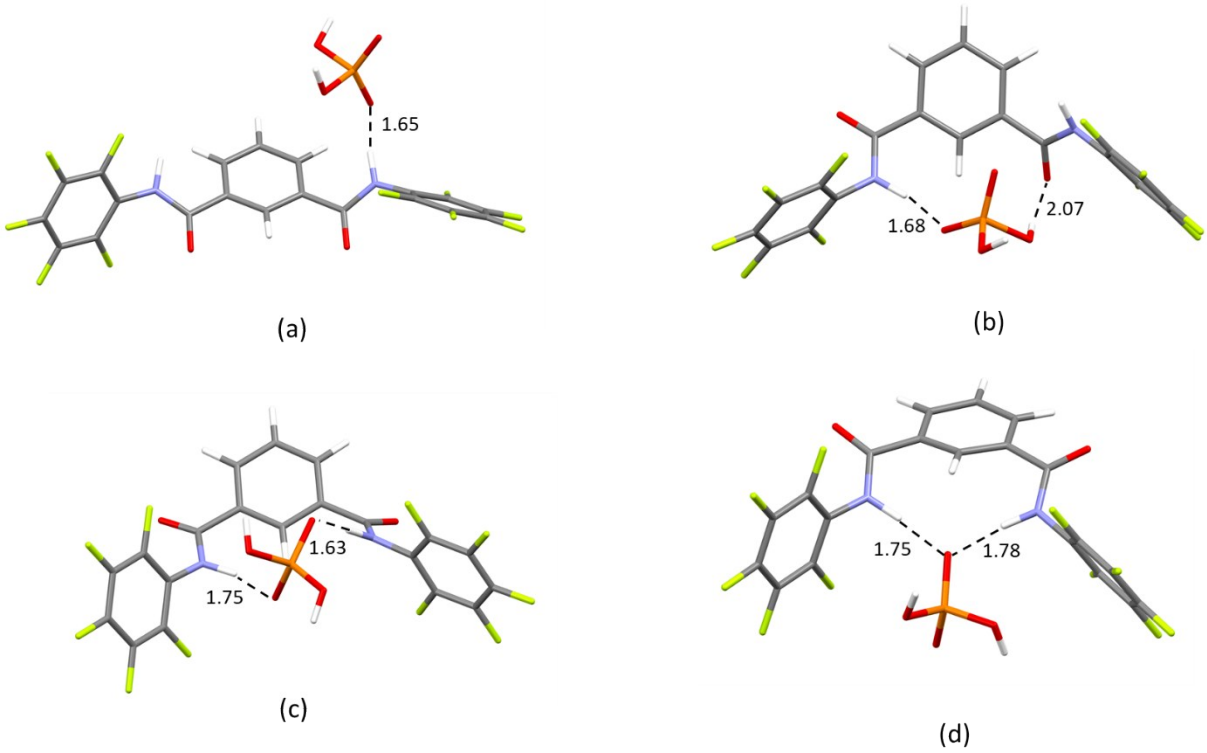

Figure S31 ***L5****/$H_2PO_4^-$ adduct:* rappresentative structures for the asymmetric and the symmetric conformers (magenta (a), light pink (b), red (c) and brown (d) points in Fig.S8). All distances in Å.

L6-benzoate adduct.

Metadynamics snapshots projected on the plane formed by the first two PCs (Fig S32 -77% of the overall variance explained) pointed out that the first component PC1 separated snapshots featured by no interactions (grey points) from frames where one (magenta and light pink points) or two H-bonds (red, brown and dark and light yellow points) occur between **L6** and the benzoate anion (positive PC1 score values). Plotting the first vs the third PCs (75% of the overall variance explained – not shown) make it possible to identify conformers where in addition to one or two H bonds, also π- π interactions are present (light pink, brown and light yellow points). Representative structures for these clusters are shown in Figure S33.

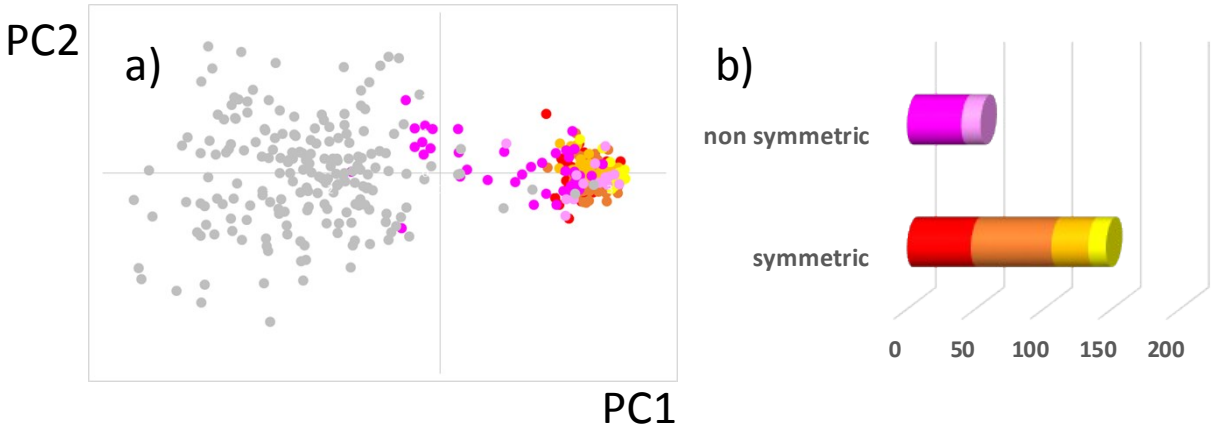

(a) (b)

Figure S32 – ***L6****/benzoate adduct* - Results from PCA analysis of frames from metadynamic trajectory: (a) PC1 vs PC2 score plot; (b) counting of the symmetric and asymmetric frames classified on the basis of the ligand/substrate H-bonds. (magenta: 1 H-bond; light pink: 1 H-bond and π-stacking interaction; red and dark yellow: 2 H-bond; brown and light yellow: 2 H-bond and π-stacking interaction; grey: no interaction)

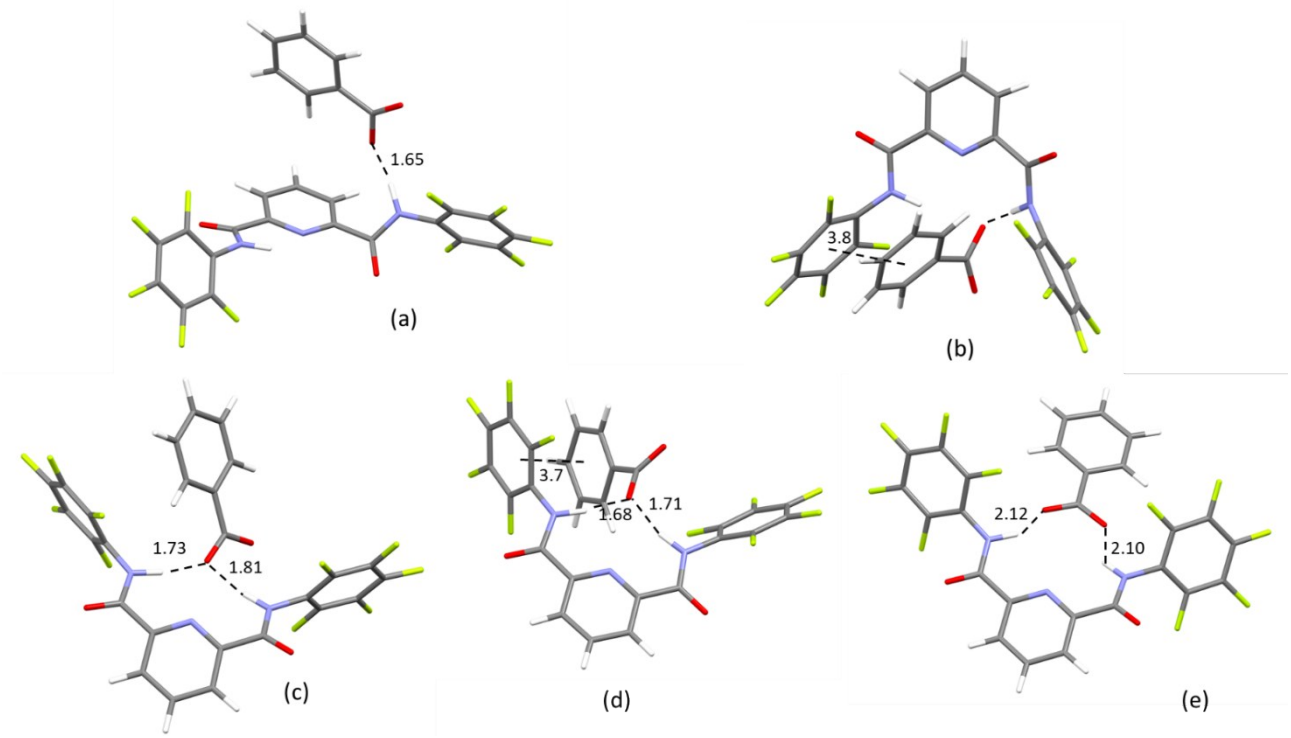

Figure S33 ***L6****/benzoate adduct:* representative structures for the magenta (a), light pink (b), red (c), brown (d) and dark yellow (e) clusters

Table S1. Atoms involved in the H-bond distances and angles definition for the **L5**/**L6**-anions (Benzoate/$H_2PO_4^-$) adducts (labelling schemes shown in Scheme S2)

	L5/benzoate	**L6**/benzoate		**L5**/$H_2PO_4^-$		**L5**/$H_2PO_4^-$
				P-OH … O=C		NH…OP
d1	Centroid Benz- Centroid Ph1	Centroid Benz- Centroid Ph1	d1	H6-O29	d5	H46-O2
d2	Centroid Benz- Centroid Ph2	Centroid Benz- Centroid Ph2	d2	H6-O47	d6	H46-O3
d3	H39-O49benz	H38-O49benz	d3	H7-O29	d7	H28-O2
d4	H39-O50benz	H38-O48benz	d4	H7-O47	d8	H28-O3
d5	H21-O49benz	H20-O49benz	a1	O1H6O29	a5	N45H46O2
d6	H21-O50benz	H20-O48benz	a2	O1H6O47	a6	N45H46O3
a3	N38H39O49	N37H38O49	a3	O4H7O29	a7	N27H28O2
a4	N38H39O50	N37H38O48	a4	O4H7O47	a8	N27H28O3
a5	N20H21O49	N19H20O48				

a6	N20H21O50	N19H20O50				

Scheme S1 – Labelling scheme used in Table S1 - Upper Panel: scheme for the **L5**/benzoate and **L6**/benzoate systems, for both systems benzoate oxygens are labelled O49 and O50; Lower Panel: scheme for the **L5**/$H_2PO_4^-$ system

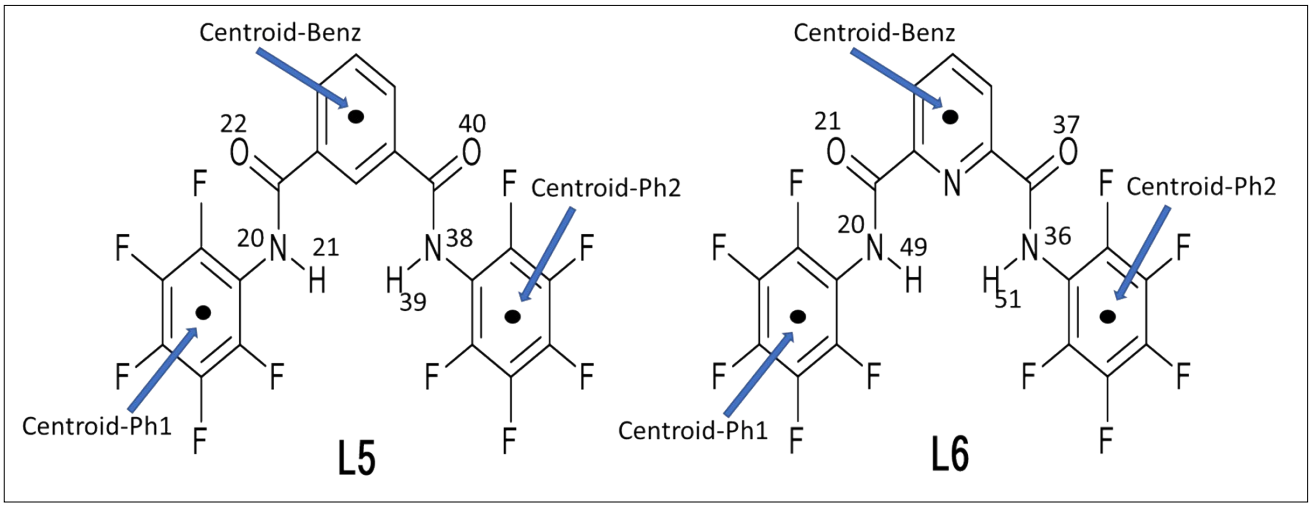

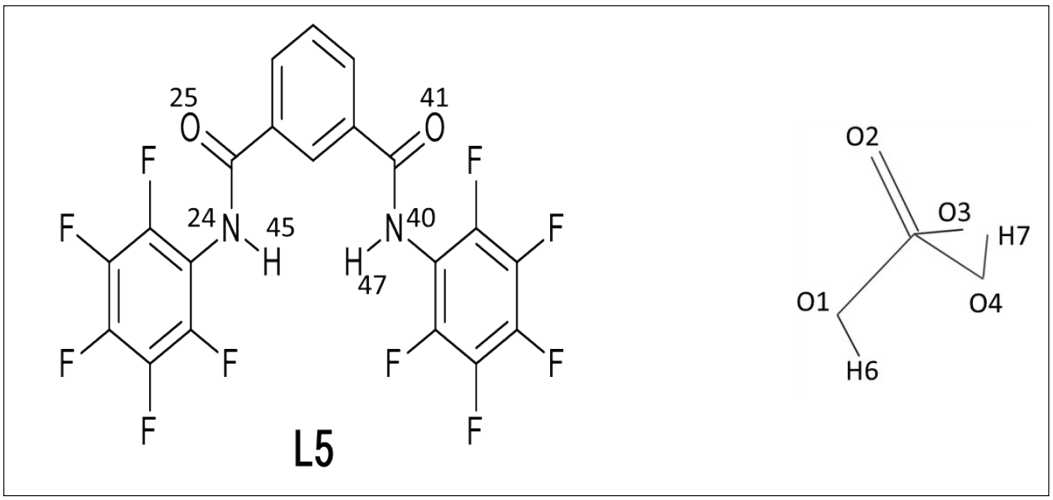

Crystallisation Experiments

Receptors **L1**-**L4** have been crystallised by slow evaporation and by slow diffusion of diethyl ether, from the following solvents: $CHCl_3$, EtOH, CH_3CN, DMSO, DMF and in a 1:1 mixture of $CHCl_3$ and MeOH. For each solvent, we attempted crystallisations of the pure receptor and of the receptor in the presence of an excess of the following anions: I^-, BzO^-, $HPpi^{2-}$, NO_3^-, $H_2PO_4^-$, Cl^-, F^-, AMP, ADP, AcO^-, $HCO_3^-$and HSO_4^-. Crystallisations in the presence of TBA^+CN^- were not attempted based on the

observation that all receptors undergo deprotonation in the presence of CN^-. Most of the crystallisations produced crystalline powders or single crystals of the precursors TBA^+salts, crystals suitable of single crystals investigation could be isolated only for **L1** (in the presence of TBA^+I^- from $CHCl_3$/MeOH 1:1), **L2** (pure receptor from $CHCl_3$) and **L4** (in the presence of the following anions F^-, AcO^-, $H_2PO_4^-$ and BzO^- all obtained by slow diffusion of diethyl ether into DMF).

Receptors **L5** has been crystallised from slow evaporation of a MeCN solution of the free receptor, while **L6** has been crystallised from a mixture of DCM and diethyl ether by solvent layering in the presence of an excess of TBAF.

X-Ray crystal data collection

L1 was collected upon a *Rigaku FRE+* rotating anode diffractometer, equipped with *VHF Varimax* confocal mirrors, an *AFC12* goniometer, *Rigaku HG Saturn724+* CCD detector and an *Oxford Cryosystems*, low-temperature device, operating at T = 100(2) K. Crystals were mounted on a *MITIGEN* holder, with perfluoroether oil. Collection strategy calculated by *CrystalClear* (Rigaku), cell parameters retrieved, and data reduction performed using *CrysAlisPro* (Rigaku Oxford Diffraction). The structure was solved with the *ShelXS* (Sheldrick, 2008) solution program using direct methods and by using *Olex2* (Dolomanov et al., 2009) as the graphical interface. The model was refined with *ShelXL* 2018/3 (Sheldrick, 2015) using full matrix least squares minimisation on F^2.

L2 was collected upon a *Rigaku FRE+* rotating anode diffractometer, equipped with *HF Varimax* confocal mirrors, an *AFC12* goniometer, *Rigaku HG Saturn724+* CCD detector and an *Oxford Cryosystems*, low-temperature device, operating at T = 100(2) K. Crystals were mounted on a *MITIGEN* holder, with perfluoroether oil. Collection strategy calculated by *CrystalClear* (Rigaku), cell parameters retrieved and data reduction performed using *CrysAlisPro* (Rigaku Oxford Diffraction). The structure was solved with the *ShelXT* (Sheldrick, 2015) solution program using dual methods and by using Olex2 (Dolomanov et al., 2009) as the graphical interface. The model was refined with *ShelXL* 2018/3 (Sheldrick, 2015) using full matrix least squares minimisation on F^2.

L4 was collected upon a *Rigaku XtaLAB AFC11* (RCD3) fine-focus (Mo) sealed X-ray tube diffractometer, equipped with a *quarter-chi* goniometer and CCD detector and an *Oxford Cryosystems*, low-temperature device, operating at T = 170(2) K. Crystals were mounted on a *MITIGEN* holder, with perfluoroether oil. Collection strategy calculated by *CrystalClear* (Rigaku), cell parameters retrieved, and data reduction performed using *CrysAlisPro* (Rigaku Oxford Diffraction).

The structure was solved with the *ShelXT* (Sheldrick, 2015) solution program using dual methods and by using Olex2 (Dolomanov et al., 2009) as the graphical interface. The model was refined with *ShelXL* 2018/3 (Sheldrick, 2015) using full matrix least squares minimisation on F^2.

L5 was collected upon a *Rigaku FRE+* rotating anode diffractometer, equipped with *VHF Varimax* confocal mirrors, an *AFC12* goniometer, *Rigaku HyPix 6000* detector and an *Oxford Cryosystems*, low-temperature device, operating at T = 100(2) K. Crystals were mounted on a *MITIGEN* holder, with perfluoroether oil. Collection strategy calculated, cell parameters retrieved, and data reduction performed using *CrysAlisPro* (Rigaku Oxford Diffraction). The structure was solved with the *ShelXT* (Sheldrick, 2015) solution program using dual methods and by using *Olex2* (Dolomanov et al., 2009) as the graphical interface. The model was refined with *ShelXL* 2018/3 (Sheldrick, 2015) using full matrix least squares minimisation on F^2.

$[L6^{2-}(TBA)_2]\cdot H_2O$ was collected upon a *Rigaku 007* rotating anode diffractometer, equipped with *HF Varimax* confocal mirrors, an *AFC11* goniometer, *Rigaku HyPix 6000* detector and an *Oxford Cryosystems*, low-temperature device, operating at T = 100(2) K. Crystals were mounted on a *MITIGEN* holder, with perfluoroether oil. Collection strategy calculated, cell parameters retrieved, and data reduction performed using *CrysAlisPro* (Rigaku Oxford Diffraction). The structure was solved with the *ShelXT* (Sheldrick, 2015) solution program using dual methods and by using *Olex2* (Dolomanov et al., 2009) as the graphical interface. The model was refined with *ShelXL* 2018/3 (Sheldrick, 2015) using full matrix least squares minimisation on F^2.

CrystalClear-SM Expert 3.1 b27, Rigaku, (2013).

CrysAlisPro Software System, Rigaku Oxford Diffraction, (2017-2020).

O.V. Dolomanov and L.J. Bourhis and R.J. Gildea and J.A.K. Howard and H. Puschmann, Olex2: A complete structure solution, refinement and analysis program, *J. Appl. Cryst.*, (2009), 42, 339-341.

Sheldrick, G.M., Crystal structure refinement with ShelXL, *Acta Cryst.*, (2015), C27, 3-8.

Sheldrick, G.M., ShelXT-Integrated space-group and crystal-structure determination, *Acta Cryst.*, (2015), A71, 3-8.

Table S2. Crystallographic parameters for structures **L1, L2, L4, L5 and [$L6^{2-}$ H_2O 2(TBA)$^+$]·{¾H_2O}**

	L1	**L2**	**L4**	**L5**	**[$L6^{2-}H_2O$ 2(TBA)$^+$]·{¾H_2O}**
Formula	$C_{20}H_{14}I_2N_2O_2$	$C_{19}H_{13}I_2N_3O_2$	$C_{20}H_{12}Cl_4N_2O_2$	$C_{20}H_6F_{10}N_2O_2$	$C_{51}H_{78.5}F_{10}N_5O_{3.75}$
Formula Weight	568.13	569.12	454.12	496.27	1011.68
Crystal system	monoclinic	monoclinic	monoclinic	monoclinic	trigonal
Space group	$P2_1/c$	$P2_1/n$	$P2_1/n$	$P2_1/m$	***P*3$_1$*c***
a /Å	19.3177(9) Å	4.2221(2)	19.0305(13)	6.9136(2)	40.29774(8)
b /Å	4.76320(10) Å	16.2083(10) Å	4.7498(3)	35.5239(12)	40.29774(8)
c /Å	22.0266(9) Å	26.3584(17)	21.7414(16)	7.4234(2)	17.08786(4)
α / º	90.00	90.00	90.00	90	90
β / º	115.372(5)	93.3100(10)	104.946(7)	96.837(3)	90
γ / º	90.00	90.00	90.00	90	120
V /Å^3	1831.27(14)	1800.78(18)	1898.7(2)	1810.21(9)	24031.42(11)
T / K	100(2)	100(2)	170(2)	100(2)	100(2)
Crystal shape	needle	needle	needle	rod	block
Crystal size / mm^3	0.22 × 0.025 × 0.001	0.37 × 0.04 × 0.02	0.231× 0.061× 0.053	0.771×0.094×0.090	0.368×0.219×0.175
Colour	light brown	colourless	colourless	colourless	colourless
Z	2	4	4	4	18
All reflns	6273	23996	17918	17034	396162
Un. reflns	5708	4122	4187	3441	28518
R_{int}	n/a	0.0387	0.0861	0.0150	0.0286

$R1_{obs}$ [I>2σ(I)]	0.0433	0.0188	0.0476	0.0338	0.0285
$R1_{all\_}$	0.0488	0.0204	0.0945	0.0389	0.0288
$wR2_{(obs)}$	0.1049	0.0448	0.0827	0.1031	0.0798
$wR2_{(all)}$	0.1081	0.0458	0.0972	0.1058	0.0801

Crystal packing of **L1.**

L1 crystallised in the monoclinic crystal system (space group $P2_1/c$), with one independent molecule in the asymmetric unit (Z'=1). As described in the article, the main supramolecular arrangement observed consists of stacks of **L1** molecules (see Fig. S20 c and d) developing along the shortest axis of the unit cell (*b*), connected via set of N-H···O hydrogen bonds (H···O distances are 1.99(4) Å and 2.04(4) Å). Within the stack, each molecule is related by inversion symmetry to molecules of an adjacent stack (see Fig. S20 e) and connected via weak C-H···…O hydrogen bonds (H···O distance is 2.46(1) Å) involving the aromatic CH in position para with respect the iodo-substituent and the carbonyl oxygen. The resulting 1-D arrangements are then packed along the *ac*-direction of the unit cell, related by inversion symmetry and, along the *a-c* direction, related by 2_1 screw axis symmetry and connected via weak I···I contacts (I…I distance 4.00(1) Å).

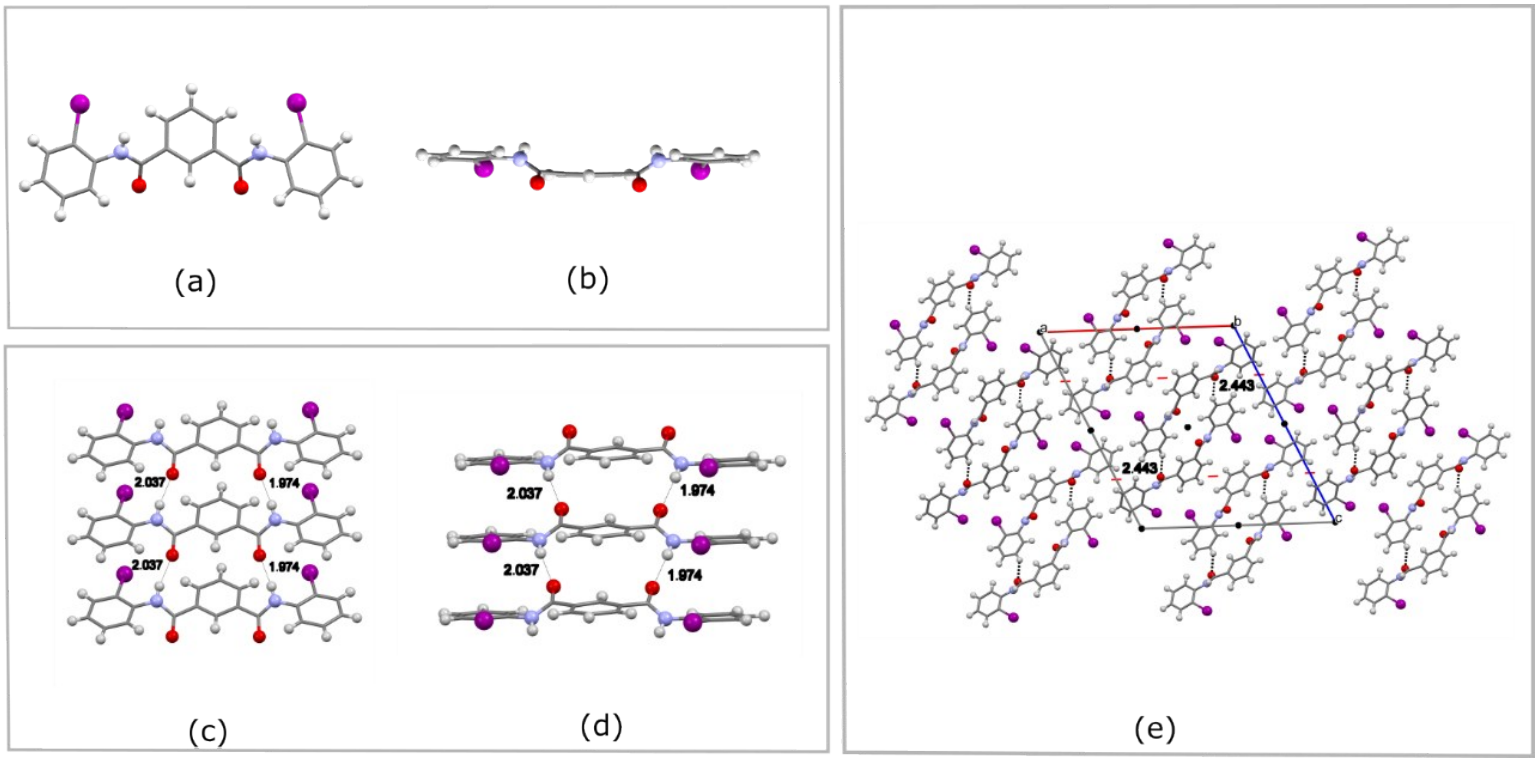

Figure S34 Crystal structure of **L1**: molecular conformation viewed along two different directions (a,b); stack of molecules viewed along two different directions (c, d); crystal packing (e).

Crystal packing of **L4.**

Like **L1**, **L4** crystallised in the monoclinic crystal system (space group $P2_1/n$), with one independent molecule in the asymmetric unit (Z'=1). The similar molecular conformation adopted by **L1** and **L4** (Figs S21 a and b) is also reflected in some structural similarities. Like in the case of **L1**, in **L4** the main supramolecular arrangement consists of a stack of receptor molecules connected via N-H…O hydrogen bonds H…O distances are 2.119(2) Å and 2.041(2) Å) and developing along the *b* direction of the packing (Figs S21 c and d). The two structures mainly differ for the different

development of this common molecular arrangement along the remaining two directions of the packing. In particular, differently to **L1**, in **L4** adjacent stacks develop along the -*ac*-direction connected via set of weak C-H···Cl (H···Cl distance are 2.911(1) Å and 2.914(1) Å) contact (see Fig S21 e). No C-H···O hydrogen bond are observed in this case.

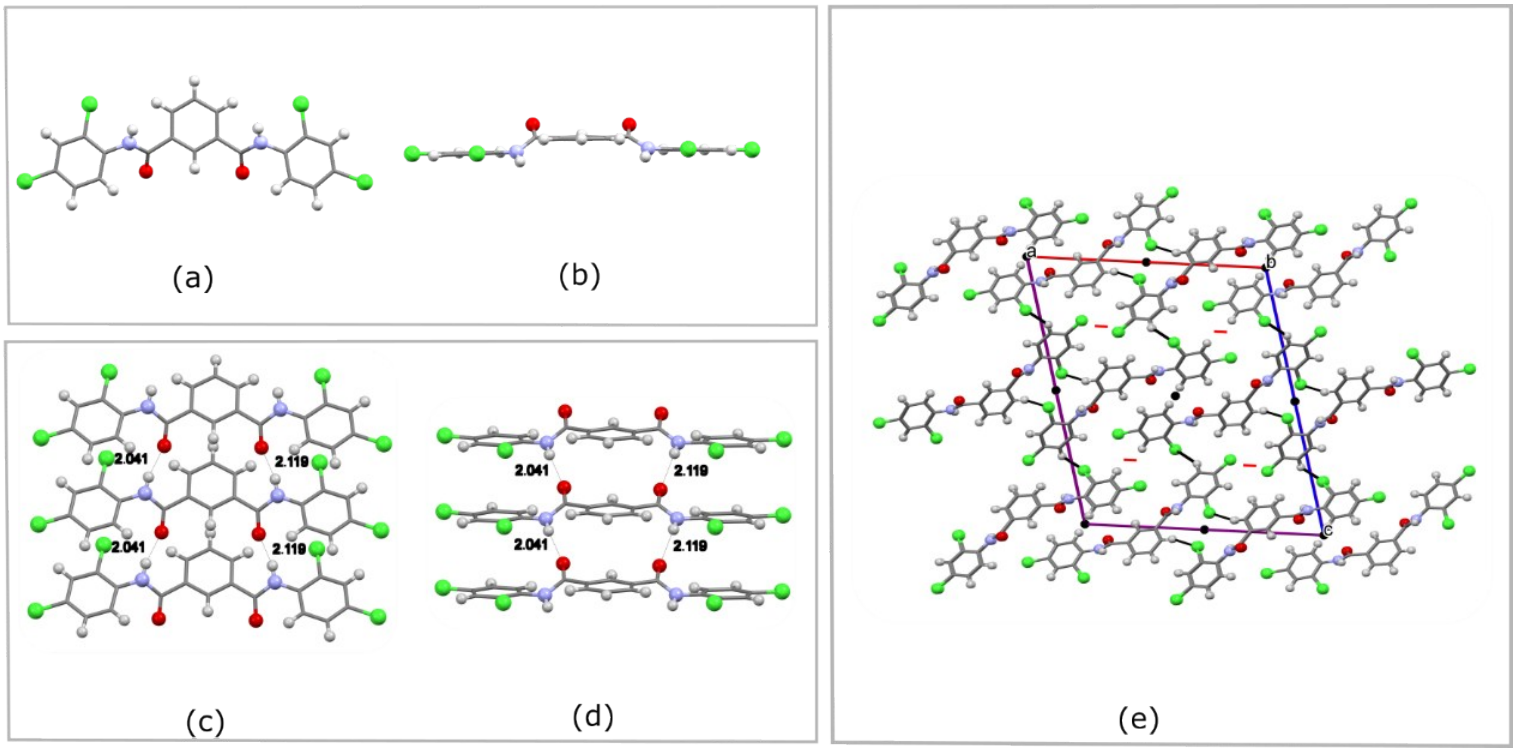

Figure S35 Crystal structure of **L4**: molecular conformation viewed along two different directions (a,b); stack of molecules viewed along two different directions (c, d); crystal packing (e).

Crystal packing of L5.

L5 crystallised in the monoclinic crystal system (space group $P2_1/m$), with an asymmetric unit consisting of two crystallographically independent half molecules (the remaining atoms related by mirror plane symmetry). The receptor molecules adopt an *anti-anti* conformation very similar to that observed in L1 and L4, with the NH-donors oriented toward the same side of the aromatic spacer and the carbonyl C=O exposed on the opposite direction, but differing for the orientation of the fluorinated aromatic rings, that in this case are oriented perpendicular with respect the plane of the aromatic spacer (Figs. S22 a and b). Like **L1** and **L4,** adjacent molecules are connected each other via N-H…O hydrogen bonds (H…O distance 2.02(2) Å) to form 1-D stacks of molecules analogous to those observed in L1 and L4 and propagating along the *ac* direction (Figs. S22 c and d). Different instances of the 1-D stack are then propagated along the *a-c* direction via set of weak C-H···F interactions (H···F distance 2.662(1) Å) and weak F···F contacts (F···F distances are 2.832(1) Å and 2.831(1) Å respectively), resulting in a 2-D molecular arrangement (Fig S22 e) that develop along the *b* direction by inversion symmetry. No relevant directional interactions are involved along this direction.

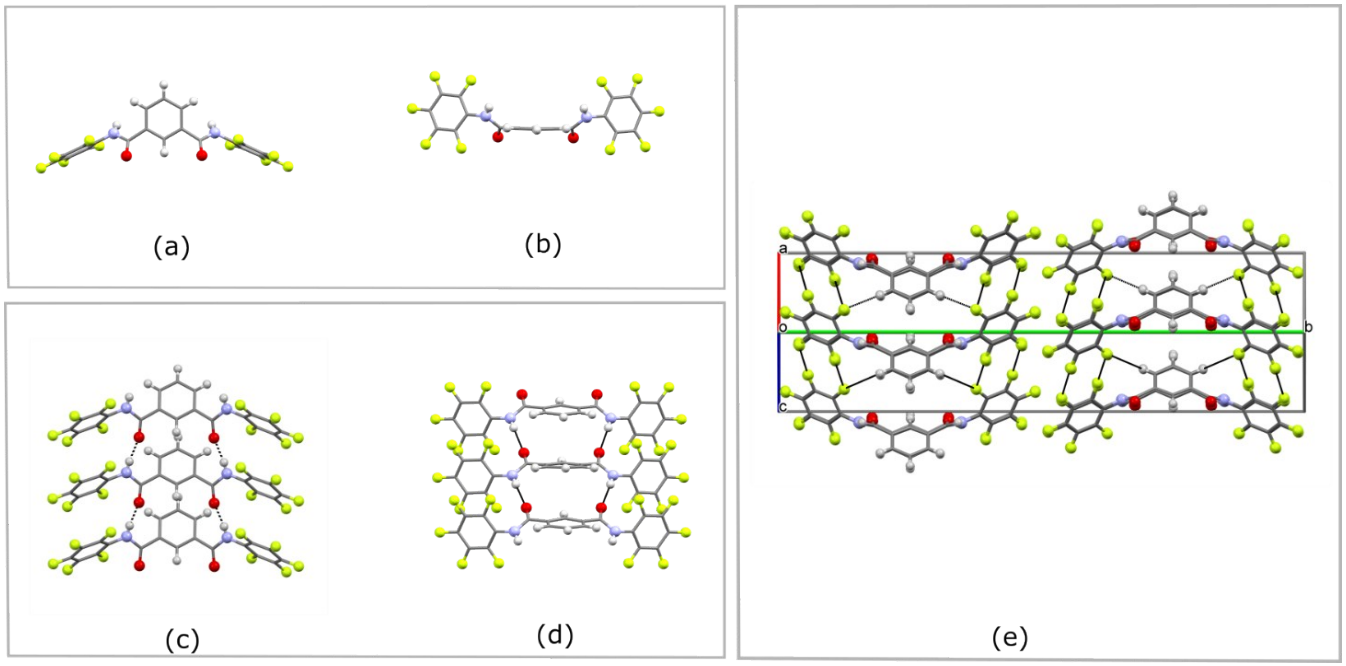

Figure S36 Crystal structure of **L5**: molecular conformation viewed along two different directions (a,b); stack of molecules viewed along two different directions (c, d); crystal packing (e).

Crystal packing of L2.

L2 crystallised in the monoclinic crystal system (space group $P2_1/c$) with one independent molecule in the asymmetric unit (Z' = 1). In this case the molecular conformation is significantly different when compared to the previous structures. In particular, **L2** adopts a *syn-syn* conformation, with the two 2-iodophenylaminocarbonyl groups oriented to the opposite side of the pyridine spacer, with NH groups pointing at the centre of a pseudo-cavity. On one side of the molecule, the iodophenyl ring lie coplanar to the pyridine spacer (Fig. S23 a). This orientation is stabilised by an intramolecular C-H···O hydrogen bond, involving the amido carbonyl oxygen and the aromatic CH of the iodo-phenyl moiety (H···O distance is 2.274(2) Å). The other iodo-phenyl ring is slightly tilted, pointing the iodo substituted group above the plane of the pyridine spacer (Fig S23 b). This

interacts with an adjacent molecule by unusually short I…I interactions (I···I distance is 3.599(1) Å), generating an infinite stack of molecules that develop along the *a* direction (Figs. S23 c and d). Each of these molecular arrangements develop along the *b* and *c* directions by inversion symmetry, interacting with equal adjacent arrangements (Fig. S23 e) via set of weak C-H···O contacts (H···O distances are 2.351(2) Å and 2.710(2) Å).

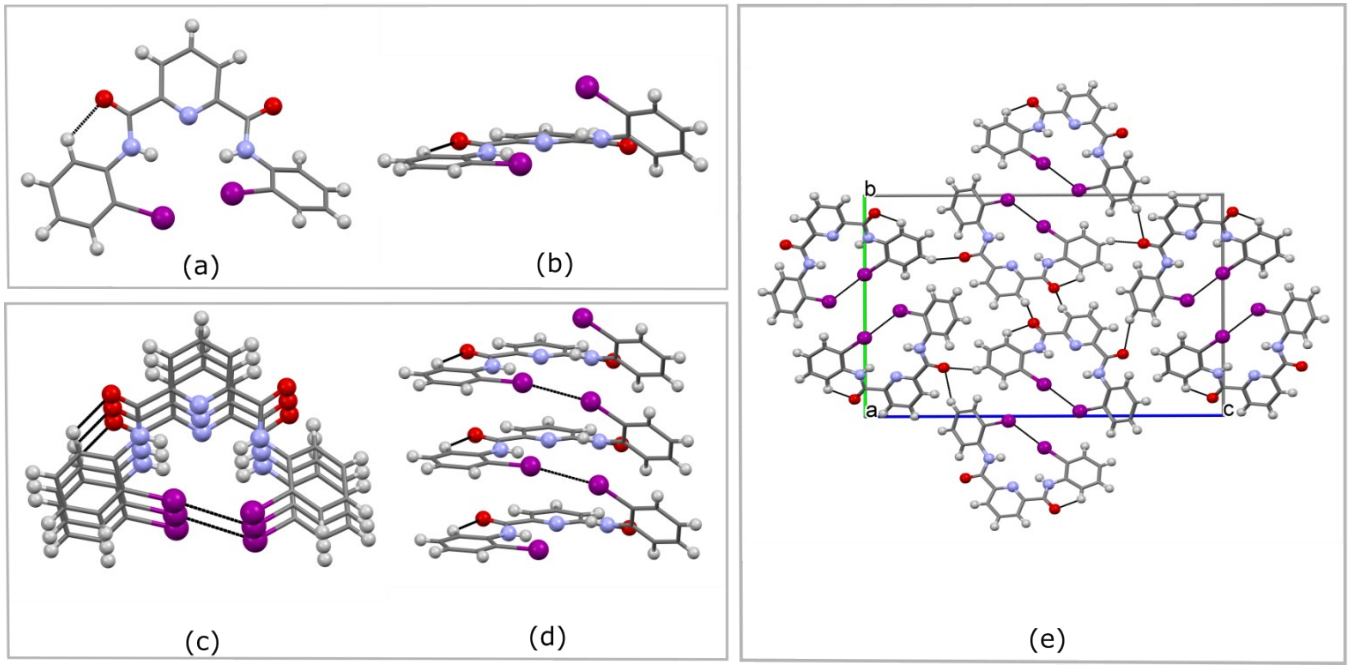

Figure S37 Crystal structure of **L2**: molecular conformation viewed along two different directions (a,b); stack of molecules viewed along two different directions (c, d); crystal packing (e).

Crystal packing of [**L6**$^{2-}$(TBA)$_2$]·H_2O**.**

Crystallisation of **L6** in the presence of TBA^+F^- from DCM by slow diffusion of diethyl ether resulted in single crystals of a hydrate salt of **L6** as the complex **[L6^{2-} H_2O 2(TBA)$^+$]·{¾H_2O}**. **[L6^{2-} H_2O 2(TBA)$^+$]·{¾H_2O}** crystallised in the trigonal crystal system (space group $P3_1c$), with an asymmetric unit consisting of three independent deprotonated receptor units, six independent TBA^+ and three independent water molecules (Z' = 3). The conformation adopted by the deprotonated **L6^{2-}** is very similar to that observed in the structure of **L2**, only differing for the different orientation of the substituted phenyl rings, that in this case are both tilted orthogonally with respect the pyridine spacer. As the consequence of this conformation the three independent **L6^{2-}** molecules feature a pseudo-cavity occupied by a molecule of water (Figs. S24 a and b), connected to the deprotonated amido N^- hydrogen bond acceptors via O-H…N^- hydrogen bonds (H…N^- distances are in the range 1.98-2.14 Å). Each of the independent **L6^{2-}** receptor units is then surrounded by TBA^+ units (Fig. S24 c and d) that interacts with the receptor via set of weak C-H···O, C-H···N and C-H···F interactions (H···O in the range 2.33-2.70 Å, H···F in the range 2.33-2.64 Å and H···N^- in the range 2.51-2.73 Å). The three independent **L6^{2-}** and the surrounding TBA^+ are then packed along the three dimensions connected by weak contacts (Fig. S24 e). The structure shows two separate solvent channels (Figs. S24 e and d) for which was not possible to refine the contents using a discrete atom model. The first channel has 16 electrons for a volume of 360 $Å^3$ while, the second channel has 28 electrons for a volume of 732 $Å^3$. This is consistent with the presence of one-quarter and one-half equivalence of a water solvent molecules per formula unit, in the 360 $Å^3$ and 732 $Å^3$ voids respectively.

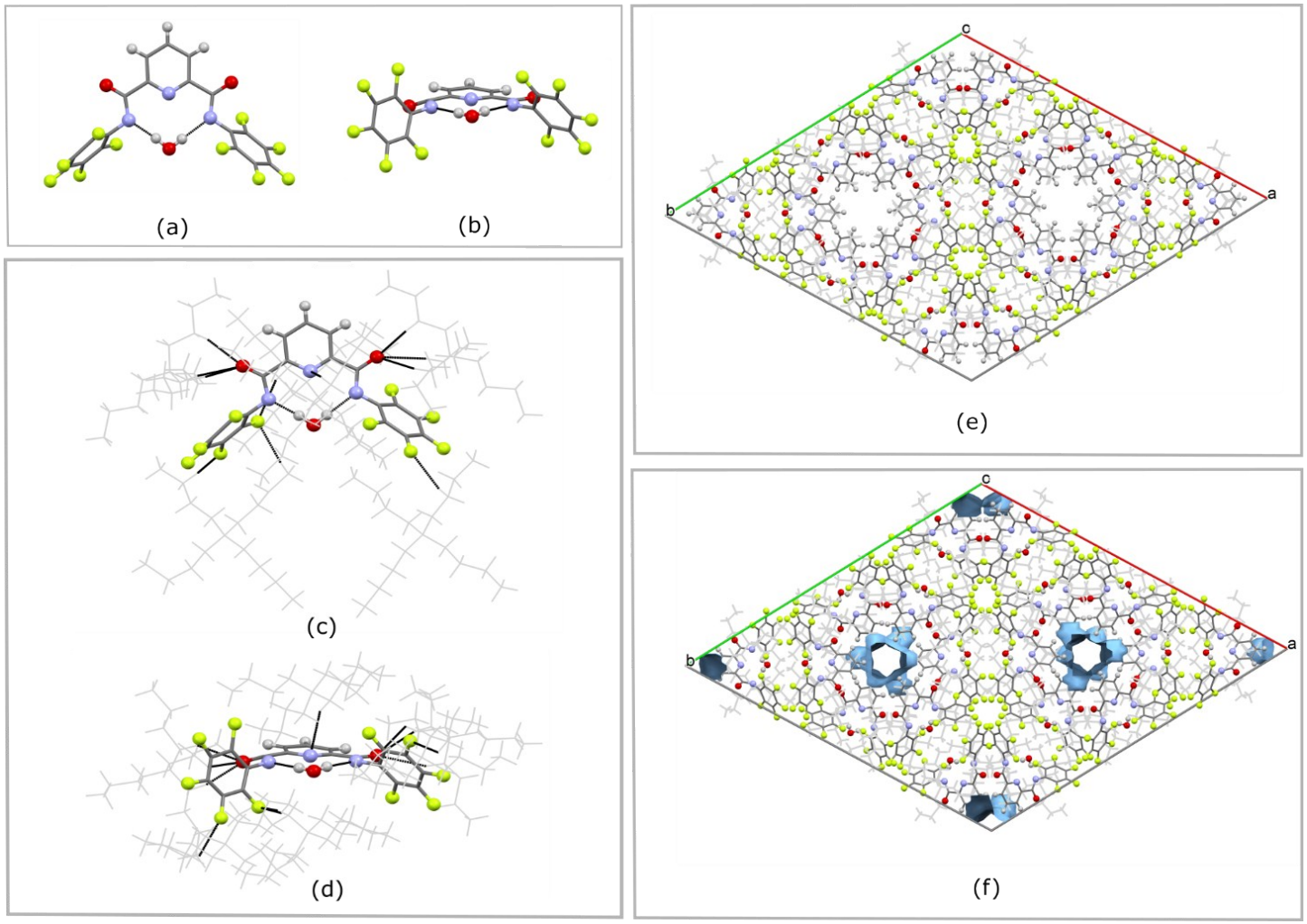

Figure S38 Crystal structure of **[$L6^{2-}$ H_2O 2$(TBA)^+$]·{¾H_2O}**. Molecular conformation and **$L6^{2-}$**- H_2O interactions viewed along two arbitrary directions (a, b); **$L6^{2-}$**- TBA^+ interactions viewed along two arbitrary directions (c, d). Two views of the unit cell showing empty channels (e) and renders of the solvent voids within **[$L6^{2-}$ H_2O 2$(TBA)^+$]·{¾H_2O} (f).**